Thesis for the Degree of Master of Engineering

Evaluation of Creep Crack Growth Rate for Modified 9Cr-1Mo Steel Using the Q^* Fracture Parameter

by

I Made Wicaksana Ekaputra

Department of Mechanical Design Engineering

The Graduate School

Pukyong National University

August 2013

Evaluation of Creep Crack Growth Rate for Modified 9Cr-1Mo Steel Using the Q^* Fracture Parameter

Q^* 파라메터를 이용한 Modified 9Cr-1Mo 강의 크리프 균열 성장 속도의 평가

Advisor: Prof. Seon-Jin Kim

by

I Made Wicaksana Ekaputra

A thesis submitted in partial fulfillment of the requirements

for the degree of

Master of Engineering

In the Department of Mechanical Design Engineering, the Graduate School

Pukyong National University

August 2013

Evaluation of Creep Crack Growth Rate for Modified 9Cr-1Mo Steel Using the Q^* Fracture Parameter

A Thesis

by

I Made Wicaksana Ekaputra

Approved as to style and content by:

Yeong-Sik Kim
(Chairman)

Woo-Gon Kim
(Member)

Seon-Jin Kim
(Member)

August, 2013

Contents

List of Figures iii

List of Tables vi

Nomenclature vii

Abstract xii

I. Introduction 1

1.1 Background and Aim 1

1.2 Thesis Outline 3

II. Theoretical Background 4

2.1 Modified 9Cr-1Mo Steel 4

2.2 Concept of Fracture Mechanics 6

2.2.1 Linear Elastic Fracture Mechanics 6

2.2.2 Elastic Plastic Fracture Mechanics 9

2.2.3 J Estimation Based on Experimentally Method 12

2.3 Creep 13

2.3.1 Creep Mechanism 14

2.4 Creep Crack Growth (CCG) 17

2.4.1 Steady State Creep 17

2.4.2 C^* Parameter 18

2.4.3 C^* Estimation Based on Experimentally Method 19

2.4.4 Q^* Parameter 19

2.4.5 Q^* Estimation Based on Activation Energy 25

III. Experimental Method 29

3.1 Experimental Procedures 29
3.2 Material Composition 29
3.3 Specimens Preparation 30
3.4 Creep Tests 30
3.5 Creep Crack Growth Tests 33
3.6 Determination of CCGR Based on Load Line Displacement 38
3.7 Determination of CCGR Based on Activation Energy 41
IV. Results and Discussion 45
4.1 Creep Test Results 45
4.2 Creep Crack Growth Rate Test Results 48
4.2.1 K Parameter 52
4.2.2 C^* Parameter 53
4.2.3 Q^* Parameter 56
4.3 Comparison of Each Parameter 61
V. Conclusions 63
References 65
Acknowledgment 69

List of Figures

Figure 2 . 1 A schematic drawing of VHTR and SFR systems. 5

Figure 2 . 2 Classification of fracture mechanics regimes on basis of dominant deformation modes. 8

Figure 2 . 3 Three modes of loading cracked body. 8

Figure 2 . 4 Coordinates and stresses around the crack tip. 8

Figure 2. 5 Definition of the *J* contour integral surrounding the crack tip. 10

Figure 2 . 6 A typical creep strain curve. 15

Figure 2 . 7 Creep ahead of the crack tip in a cracked body. 15

Figure 2 . 8 Creep mechanisms. 16

Figure 2 . 9 Schematic deformation mechanism map. 16

Figure 2 . 10 Schematic representation of (a) small scale (b) transition and (c) widespread creep conditions. 17

Figure 2 . 11 Schematic illustration of evaluating method by *log da/dt* vs *log* $\dot{\delta}$ projection $t_i < t_{t.}$ [5]. 22

Figure 2 . 12 Schematic illustration of evaluating method by *log da/dt* vs *log* $\dot{\delta}$ projection $t_t < t_i < t_{s.}$ [5]. 22

Figure 2 . 13 Schematic illustration of evaluating method by *log da/dt* vs *log* $\dot{\delta}$ projection $t_s < t_{i.}$ [5]. 23

Figure 2 . 14 Comparison of the CCGR characteriscs between inner and outer parts of turbine rotor as estimated by the Q^*_{INN} parameter [3]. 24

Figure 2 . 15 The CCGR estimated by the C^* parameter (CrMoV CT specimen) [3]. 24

Figure 2 . 16 Comparison of characteristics of the CCGR between CrMoV steel and SUS 304 steel as estimated by the C^* parameter [3]. 25

Figure 2 . 17 Ilustration of the activation energy. 26

Figure 2 . 18 Interestial diffusion. 27

Figure 2 . 19 Substitutional diffusion. 27

Figure 3. 1 Dimensions of ½ CT specimen. 31
Figure 3 . 2 Shape of the CT specimen with the side grooves. 31
Figure 3 . 3 Dimensions of the creep specimen. 32
Figure 3 . 4 Appratus of creep test machine. 32
Figure 3 . 5 A schematic illustration of CCG testing apparatus. 37
Figure 3 . 6 Lead position for measuring potential drop in CT specimen. 37
Figure 3 . 7 Schematic illustration for Arrhenius-type relation [3]. 43
Figure 3 . 8 Schematic relationship between activation energy and *K* [3]. 43
Figure 3 . 9 Schematic relationship between *n* and absolute temperature [3]. 44
Figure 3 . 10 Schematic relationship between gross stress and *K* [3]. 44

Figure 4 . 1 Determination of creep constants at 550^{o}C. 47
Figure 4 . 2 Determination of creep constants at 600^{o}C. 48
Figure 4 . 3 Validity criteria corelating to the CCG data with the parameter at 550^{o}C. 49
Figure 4 . 4 Validity criteria corelating to the CCG data with the parameter at 600^{o}C. 49
Figure 4 . 5 Plot of LLD vs. time at 550^{o}C. 50
Figure 4 . 6 Plot of crack length vs. time at 550^{o}C. 50
Figure 4 . 7 Plot of LLD vs. time at 600^{o}C. 51
Figure 4 . 8 Plot of crack length vs. time at 600^{o}C. 51
Figure 4 . 9 Determination of the CCGR with *K* parameter. 52
Figure 4 . 10 Plot of CCGR vs. C^* at 550^{o}C including transition time. 54
Figure 4 . 11 Plot of CCGR vs. C^* at 600^{o}C including transition time. 55

Figure 4 . 12 Result of CCGR law by the C^* at 550°C excluding transition time. 55

Figure 4 . 13 Result of CCGR law by the C^* at 600°C excluding transition time. 56

Figure 4 . 14 Determination of activation energy at a specific value of stress. 57

Figure 4 . 15 Relationship between the CCGR and inverse absolute temperature. 58

Figure 4 . 16 Relationship between the creep exponent and inverse of absolute temperature. 58

Figure 4 . 17 Relationship between the apparent activation energy *U* and the *K* parameter. 59

Figure 4 . 18 Relationship between the *K* and gross stress at a specific CCGR. 59

Figure 4 . 19 Determination of the CCGR by the Q^* parameter under various loads at 550°C and 600°C. 61

Figure 4 . 20 Determination of the CCGR by the C^* parameter under various loads at 550°C and 600°C. 62

List of Tables

Table 3 . 1 Chemical composition of modified 9Cr-1Mo steel (wt. %)...................... 29

Table 3 . 2 The CCG test conditions and crack size measurements at 550^{o}C. 36

Table 3 . 3 The CCG test conditions and crack size measurements at 600^{o}C. 36

Table 4 . 1 Mechanical properties of modified 9Cr-1Mo steel under various loads at 550^{o}C and 600^{o}C. 46

Table 4 . 2 Creep rate results at 550^{o}C.. 46

Table 4 . 3 Creep rate results at 600^{o}C.. 47

Nomenclature

a	Crack length, [mm]
a_e	Effective crack length, [mm]
a_{mf}	Measured crack length, [mm]
a_0	Initial crack length measurement, [mm]
a_{pf}	Predicted crack length, [mm]
$\dot{a}$, da/dt	Creep crack growth rate, [mm/h]
A	Power law creep (secondary creep) coefficient, [$MPa^{-n}h^{-1}$]
A_c	Crack area, [mm^2]
A^*	Constant depending on σ_g
B	Specimen thickness, [mm] or constant coefficient in creep crack growth correlation with $C^*$and Q^*
B_n	Specimen net section thickness between side-grooves, [mm]
C_t	Small scale creep and transition creep parameter, [$Nmm^{-1}h^{-1}$]
C^*	Steady state creep characterising parameter, [$Nmm^{-1}h^{-1}$]
C_t^*	Experimentally determined value of C^* at test time t, [$Nmm^{-1}h^{-1}$]
C^*_{exp}	Experimentally determined value of C^*, [$Nmm^{-1}h^{-1}$]
C^{*CMOD}	C^* from crack mouth opening displacement measurements, [$Nmm^{-1}h^{-1}$]
C^{*LLD}	C^* from load line displacement measurements, [$Nmm^{-1}h^{-1}$]
D	Coefficient in Ramberg-Osgood's equation creep crack growth correlation with $C^*$and Q^*
E	Young's modulus, [GPa]
E'	Effective Young's Modulus, [GPa]
$f_{ij}(\theta)$	Angular functions
H	Non-dimensional function of specimen geometry and N

H^{CMOD}	Non-dimensional function of specimen geometry and N *(or n)* relating crack mouth opening displacement to J_p *(or* C^**)*
H^{LLD}	Non-dimensional function of specimen geometry and N (or *n)* relating load line displacement to J_p (or C^*)
J -integral	Elastic-Plastic fracture mechanics parameter, [N/mm]
J_e	Elastic contribution to J, [N/mm]
J_p	Plastic contribution to J, [N/mm]
K	Linear elastic stress intensity factor, [MPa.m$^{1/2}$]
m	Creep stress exponent correlation with Q^*
n	Creep stress exponent correlation with C^*
n_j	Outward normal vector to the crack tip contour
N	Stress dependence exponent of plastic deformation
P	Load, [N]
q	Material constant in the relationship $\dot{a} = D\,(C^*)^q$
Q^*	Exponent of the exponential function in the thermal activation process
r	Radial distance from crack tip, [mm]
R	Gas constant, [J.mol^{-1}.K^{-1}]
ds	Element along the crack tip contour Γ
t	Time, [h]
t_a	Time to the minimum crack growth rate, [h]
t_{ai}	Time to the starting of the constant rate crack growth, [h]
t_i	Time to crack initiation, [h]
t_t	Time to the termination of transient creep, [h]
t_T	Transition time from small scale creep to widespread creep conditions, [h]
t_s	Time to the termination of steady state creep or starting of accelerating creep, [h]

T	Temperature, [K]
T_i	Traction vector, [N]
T_m	Melting temperature, [K]
u_i	Displacement vector, [mm]
$\dot{u}_i$	Displacement rate vector, [mm/h]
U	Potential energy (for non-linear elastic material), [J] or apparent activation energy for crack extension, [KJ.mol^{-1}]
V, V_0, V_f	Instantaneous, initial and final potential drop (PD) readings, [volt]
W	Specimen width (or half width), [mm] or strain energy density, [N.mm^{-2}]
W_s^*	Strain energy density rate, [N.mm^{-2}h^{-1}]
y_o	A half distance between output potential leads, [mm]
Y	Non-dimensional geometric function in expression for K
V_C, Δ_C	Component of displacement due to creep strains, [mm]
$dV_c/dt, \dot{\Delta}_C$	Component of displacement rate due to creep strains, [mm/h]
Δ^{CMOD}	Crack mouth opening displacement, [mm]
V_{el}, Δ_{el}	Component of displacement due to elastic strains, [mm]
$dV_{el}/dt, \dot{\Delta}_{el}$	Component of displacement rate due to elastic strains, [mm/h]
V, Δ, Δ^{Exp}	Displacement by experimental, [mm]
$dV/dt, \dot{\Delta}, \dot{\Delta}^{Exp}$	Displacement rate by experimental, [mm/h]
Δ^{LLD}	Load line displacement, [mm]
V_{pl}, Δ_{pl}	Component of displacement due to plastic strains, [mm]
$dV_{pl}/dt, \dot{\Delta}_{pl}$	Component of displacement rate due to plastic strains, [mm/h]
$\dot{\delta}$	Load line displacement rate, [mm/h]

ε	Strain
$\dot{\varepsilon}_{ss}$	Strain rate at steady state condition, [1/h]
ε_{ij}	Strain tensor
ε_{c}	Component of strain due to creep
ε_{e}	Elastic component of strain
ε_{p}	Plastic component of strain
$\dot{\varepsilon}$	Strain rate, [1/h]
$\dot{\varepsilon}_{min}$	Secondary (or minimum) creep strain rate, [1/h]
η	Factor relating J or C^* to load and displacement measurements
η^{CMOD}	Factor relating J or C^* to load and crack mouth opening displacement
η^{LLD}	Factor relating J or C^* to load and load line displacement
Γ	Crack tip contour
σ	Stress, [MPa]
σ_{ij}	Stress tensor, [MPa]
σ_{net}	Section stress net, [MPa]
σ_{ys}	Yield stress, [MPa]
θ	Angular position
ν	Poisson's ratio
CCG	Creeep Crack Growth
CCGR	Creep Crack Growth Rate
CMOD	Crack Mouth Opening Displacement
CT	Compact Tension
CTOD	Crack Tip Opening Displacement
DCPD	Direct Current Potential Drop
EPFM	Elastic-Plastic Fracture Mechanics
LEFM	Linear-Elastic Fracture Mechanics

LLD	Load Line Displacement
LVDT	Linear Variable Differential Transformer
NLFM	Non-Linear Fracture Mechanics
SFR	Sodium-Cooled Fast Reactor
SIF	Stress Intensity Factor
SSC	Small Scale Creep
SSY	Small Scale Yield
TDFM	Time-Dependent Fracture Mechanics
VHTR	Very High Temperature Reactor

Evaluation of Creep Crack Growth Rate for Modified 9Cr-1Mo Steel Using the Q^* Fracture Parameter

I Made Wicaksana Ekaputra
Department of Mechanical Design Engineering, The Graduate School,
Pukyong National University

Abstract

The modified 9Cr-1Mo (ASME Grade 9Cr-1Mo, Gr. 91) steel is favoured structural materials for Generation-IV reactor systems, such as reactor pressure vessels in very high temperature reactor (VHTR) and steam generators, intermediate heat exchangers (IHX), and primary hot pipes in sodium-cooled fast reactor (SFR).

The selection of the modified 9Cr-1Mo is based primarily on its low thermal expansion coefficient and high resistance to stress corrosion cracking in water-steam systems compared to austenitic stainless steels. In particular, it also has better mechanical properties at elevated temperatures compared to alternate 2.25 Cr-1Mo steel. Since their structural components are designed to last for up to 60 years at elevated temperature, above all, the creep and creep crack growth (CCG) behaviors should be evaluated for a design application.

The material that is operated under high temperature and/or high stress during the long service life may generate localized creep damage, propagating cracks, and ultimately causing fracture. A significant portion of the component lifetime will be spent in crack propagation. Therefore, an accurate assessment of crack propagation owing to the creep crack growth rate (CCGR) is required for the design and safety

considerations. To do so, each characteristics of the fracture parameters such as K, C^*, and Q^* should be investigated and compared to define the CCGR behavior.

In this study, a series of creep and creep crack growth tests was carried out on the modified 9Cr-1Mo steel under various loads at 550°C and 600°C. The CCGR behavior of the modified 9Cr-1Mo steel was evaluated using the three fracture parameters of K, C^*, and Q^*, and their characteristics were compared and discussed.

Results showed that the Q^* parameter could reasonably evaluate the CCGR by a simple monotical linear function without a dual value due to nose in the early stage of creep crack growth curve, while the C^* parameter revealed the dual value in the early stage. In the scattered data from early stage to acceleration stage, the Q^* parameter was found to be superior to the C^* parameter, while the K parameter was the largest scatter and there was no systematic trend among each series of tests. It was identified that the Q^* parameter was regarded as an independent parameter, whereas the C^* was regarded as a dependent parameter that depends on creep deformation rate, which is a function of stress, temperature, specimen shape, and activation energy of deformation, etc.

I. Introduction

1.1 Background and Aim

High-chromium modified 9Cr-1Mo steel (ASME Grade 9Cr-1Mo, Gr. 91) is favoured structural materials for Generation-IV reactor systems, such as reactor pressure vessels in very high temperature reactor (VHTR) and steam generators, intermediate heat exchangers (IHX), and primary hot pipes in sodium-cooled fast reactor (SFR).

The selection of modified 9Cr-1Mo steel is preliminarily based on its low thermal expansion coefficient and high resistance to stress corrosion cracking in water-steam systems compared to austenitic stainless steels. It also has better mechanical properties at elevated temperatures compared to alternate 2.25 Cr-1Mo steel [1-2]. Since their structural components are designed to last for up to 60 years at elevated temperature, the creep and creep crack growth (CCG) behaviors owing to creep damage during long service life should be evaluated for a design application.

Generally, the heat-resistance steel, which is operated under high temperature and/or high stress during the long service life, may generate localized creep damage, propagating cracks, and ultimately causing fracture. A significant portion of the component lifetime will be spent in crack propagation. Therefore, an accurate assessment of crack propagation owing to the creep crack growth rate (CCGR) is required for the design and safety considerations [2].

In order to consider field parameters for characterizing crack growth ahead of crack tip at elevated temperature, various fracture mechanics parameters such as the K, J, C^*, C_t, and Q^* have been proposed by Rice, Nikbin, Webster, Saxena, and Yokobori et, al [3-17]. The K parameter is used for characterizing the crack tip stress and strains for elastic region, and the J parameter is used for plastic region. In addition, in case of the presence of the creep deformation, the K and J-integral are not valid crack tip parameter. As long as the “stress relaxation” or the creep region is small, the K and J are still good far field parameters outside of the creep zone. However, within the creep zone, the stress field is not uniquely related to the K or J which in unlike the situation in the subcreep temperature regime. Therefore, to characterize crack growth under creep conditions, the C^* and C_t parameters are needed. The C^* and C_t parameters as time-dependent fracture mechanics (TDFM) have been used well, and the C^* parameter have been more commonly used than the C_t parameter. However, there is a little difference between the C^* and C_t parameters, namely, the C^* parameter is under the steady state creep conditions which the crack tip stress no longer varies with time. And the C_t parameter is the total of the transient creep conditions (small scale creep + transition creep) and the steady state creep conditions. However, the C^* and C_t parameters are still lack in a physical meaning for estimation of the creep crack growth of cracked body.

In these circumstances, Yokobori et al. have proposed newly the Q^* parameter as a better parameter compared with the C^* and C_t parameters in the creep crack estimation. They have reported that incidentally, the C^* parameter depends on creep deformation rate, which is a function of stress, temperature, specimen shape, and activation energy of deformation, etc. The differences of the CCGR characteristics caused by various conditions are controlled by the creep deformation rate, so it seems reasonable to estimate the CCGR in one band by using the C^* parameter. It is therefore difficult to define the changes of the CCGR characteristics due to material properties, stress, temperature, and specimen shape that prevent the application of the C^* parameter to the actual CCGR [4-5].

A parameter for applying to actual the CCGR must: (i) indicate the physical mechanism, which can be estimated by input conditions such as stress, temperature and specimen shape; (ii) accurately distinguish between the variations of material properties, such as activation energy, and estimate the change of characteristics represented by the acceleration of reduction of the CCGR [3]. The Q^* parameter can be defined as the exponent of the exponential in the thermal activation process equation. Yokobori et al. reported from experimental results that the Q^* parameter could reasonably evaluate the CCGR by a simple monotical linear function without a dual value due to nose in the early stage of the CCG curve, and it could be regarded as an independent parameter that could distinguish between the variations of material properties. Therefore, applicability of the Q^* parameter should be identified to define the CCGR of modified 9Cr-1Mo steel.

In this study, the Q^* parameter was applied to evaluate the CCGR behavior for the modified 9Cr-1Mo steel. To calculate the Q^* value, the creep and CCG data were obtained from a series of creep and CCG tests under various applied loads at 550°C and 600°C. Based on experimental results, the Q^* CCGR law in addition to the K and C^* parameters was obtained, and its characteristic was compared and discussed.

1.2 Thesis Outline

Chapter 2 contains the basic explanation of fracture mechanics concept, material review and several parametric methods for characterizing the CCGR behavior.

Chapter 3 contains the detail procedures of the creep and CCG tests, and also the apparatuses used in the experiment.

Chapter 4 describes the results of experiment and calculation of the CCGR by using the K, C^*, and Q^* parameters.

Chapter 5 gives the conclusions based on the results drawn in this research.

II. Theoretical Background

2.1 Modified 9Cr-1Mo Steel

To use the hot dust material in the SFR system, according to the ASTM A-826, the 9Cr-1Mo grade ferritic steel shall conform to the applicable chemical requirements. The content (wt. %) has a carbon range 0.08 ~ 0.12, a silicon range 0.2 ~ 0.5, a manganese range 0.3 ~ 0.6, a phosphorus maximum value of 0.02, a sulfur maximum value of 0.01, a nickel maximum value of 0.4, a chromium range 8 ~ 9.5, a molybdenum range 0.85 ~ 1.05, a vanadium range 0.18 ~ 0.25, an aluminium maximum value of 0.04, a nitrogen range 0.03 ~ 0.07, and a niobium range 0.05 ~ 0.11 [18].

The modified 9Cr-1Mo steel is a modified alloy similar to conventional 9Cr-1Mo grade ferritic steel. Modifications include additions of vanadium, niobium, and nitrogen, as well as lower carbon content. This alloy is much more resistant to thermal fatigue than austenitic stainless steels because of its lower thermal expansion coefficient (at least 30% lower) and higher thermal conductivity. This alloy provides good mechanical properties at elevated temperature when produced and heat treated to form the proper microstructure. This microstructure includes stable submicroscopic vanadium-rich $M_{23}C_6$ particles that contribute to high-temperature strength and creep resistance [1].

Currently, the modified 9Cr -1Mo steel is being considered as the structural components for a Generation-IV reactors, such as reactor pressure vessels in the VHTR and steam generators, intermediate heat exchangers (IHX), and primary hot pipes in the SFR, as shown in Fig. 2.1. Since their structural components are designed to last for up to 60 years at elevated temperature, the creep and creep crack growth (CCG) behaviors are very important, and also the CCG data are needed for a design application [1].

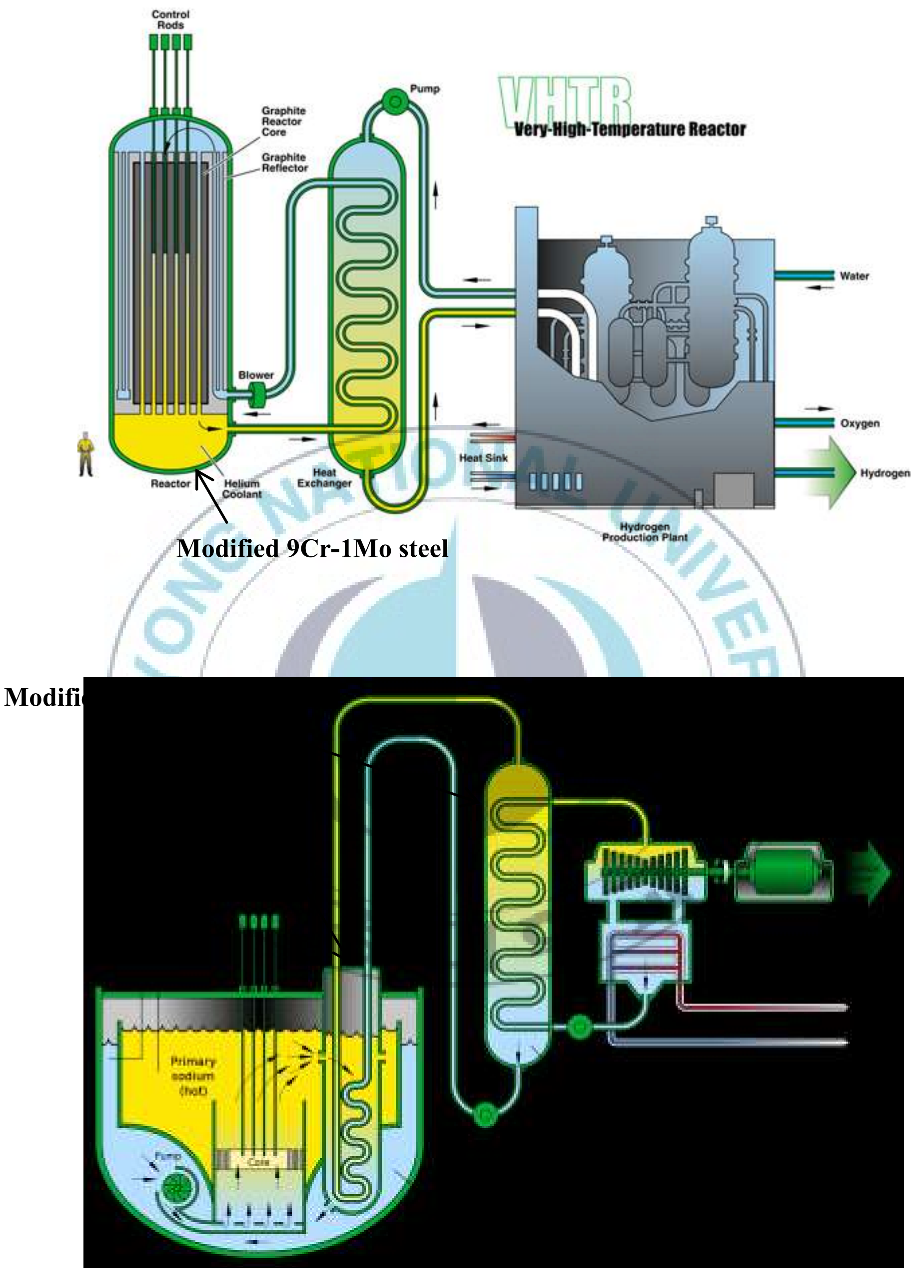

Figure 2 . 1 A schematic drawing of VHTR and SFR systems.

2.2 Concept of Fracture Mechanics

Fracture mechanics has been classified into linear-elastic fracture mechanics (LEFM), elastic-plastic fracture mechanics (EPFM), and time-dependent fracture mechanics (TDFM) regimes. Its classification is based on the dominant operating deformation modes in the cracked bodies, as shown in Fig. 2.2. When the stress-strain and the load-displacement behaviors are linear, the LEFM can be used, and a relevant crack tip parameter becomes the stress intensity parameter (SIF) K. In this regime, the plastic zone is small in comparison to the crack size and other pertinent dimensions of the cracked body. When dominanly linear conditions can no longer be ensured due to large-scale plasticity, the EPFM is used, and the relevant crack tip parameter is the J-integral. Finally, when the stress-strain and the load-displacement behaviors are time-dependent due to either dynamic loading or due to time-dependent creep, the concept of the TDFM must be used. When the loading rates are very high, the crack tip stresses are influenced by shear waves and by kinetic energy considerations which are neglected in a conventional LEFM. Similarly, when time-dependent creep occurs, the crack tip stress and deformation fields change with time. The crack tip parameter in such case is the C_t parameter and C^* parameter [12].

2.2.1 Linear Elastic Fracture Mechanics

The presence of a crack in a component of structure causes the local stresses to be dramatically increased in the region of the crack tip. In a cracked or nocthed body, the local stress to the defect is significantly higher than the remote stress in the body. The stress in the vicinity of the sharp crack in the body under linear elastic conditions may be described using the K parameter. It can refer to three distinct modes of crack surface deformation. They are mode I (opening), mode II (edge-sliding), mode III (tearing), as shown in Fig. 2.3 [19].

This investigation will be concerned only with fracture under mode I loading since this is the most common case which causes crack extension in components. For a linear-elastic material, the stress field in the vicinity of a sharp crack σ_{ij}, may be written as [20],

$$\sigma_{ij} = \frac{K}{\sqrt{2\pi r}} f_{ij}(\theta) \tag{2.1}$$

where K is the linear elastic stress intensity factor, r is the radial coordinate from the crack tip, as shown in Fig. 2.4, and f_{ij} is a non-dimensional function of angle, given by

$$f_{xx}(\theta) = \cos\frac{\theta}{2}\left[1 - \sin\frac{\theta}{2}\sin\frac{3\theta}{2}\right] \tag{2.2}$$

$$f_{yy}(\theta) = \cos\frac{\theta}{2}\left[1 + \sin\frac{\theta}{2}\sin\frac{3\theta}{2}\right] \tag{2.3}$$

$$f_{xy}(\theta) = \cos\frac{\theta}{2}\sin\frac{\theta}{2}\cos\frac{3\theta}{2} \tag{2.4}$$

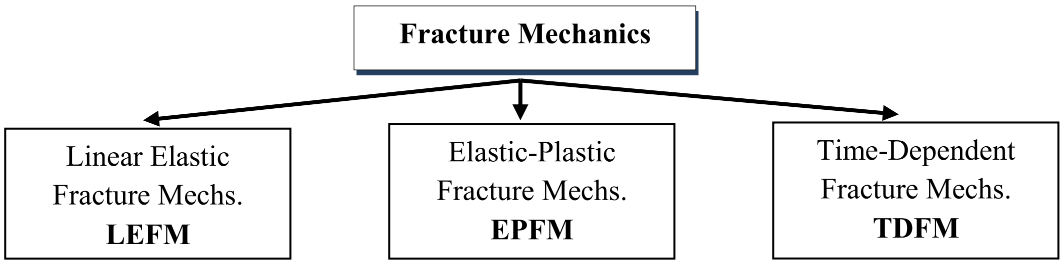

Figure 2 . 2 Classification of fracture mechanics regimes on basis of dominant deformation modes.

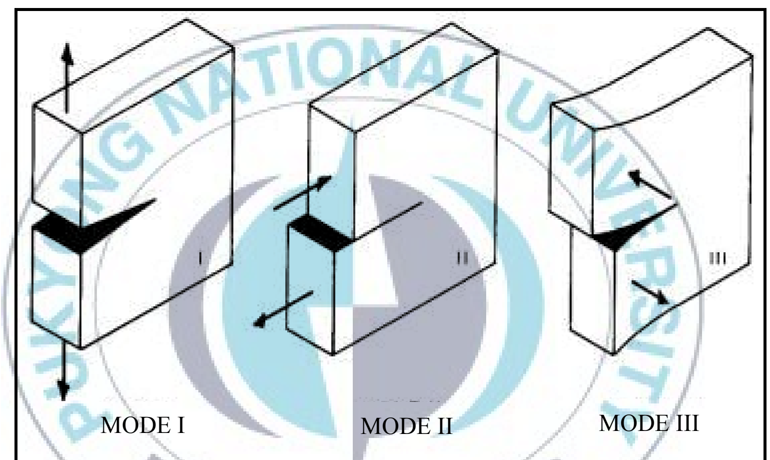

Figure 2 . 3 Three modes of loading cracked body.

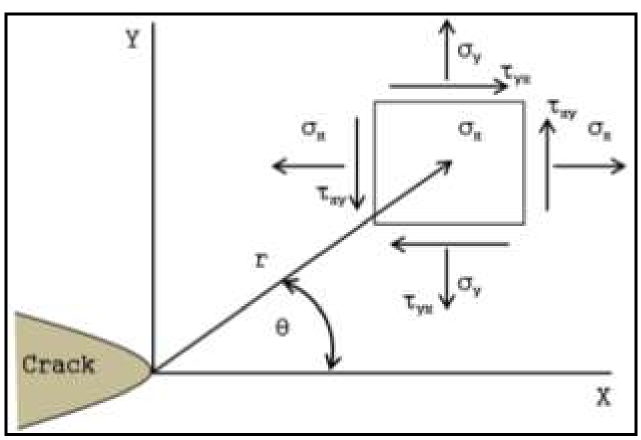

Figure 2 . 4 Coordinates and stresses around the crack tip.

In addition, Eq. (2.1) predicts that the stresses tend to infinity $r \rightarrow 0$, giving a crack tip singularity. This is not representative of real behavior since plastic deformation around the crack tip keeps the stress finite. For most material, plastic deformation occurs where the stress exceeds the yield stress of the material, producing a plastic zone close to the crack tip. Consequently, the stress intensity factor is an adequate parameter providing that the plastic zone is small enough compared to the K dominant stress field area. This is called small scale yielding condition (SSY) or crack tip plasticity.

Finally, assuming a linear elastic body, the K is proportional to the applied load. For instance, for the case of an infinite body containing a finite center crack length a, perpendicular to uniaxial stress field σ, (Fig. 2.4), the K is given the expression [21]:

$$K = \sigma\sqrt{a}Y(a/W) \tag{2.5}$$

where σ is a representative stress, $Y(a/W)$ is a non-dimensional function of crack size and component dimensions. It includes different terms such as magnification factors, bulging corrections factors, and finite width corrections.

2.2.2 Elastic Plastic Fracture Mechanics

The LEFM was originally developed to describe crack growth and fracture under essentially elastic conditions. However, under the situations where the material is ductile, and thus substantial plastic deformation occurs, the LEFM is no longer applicable, and this led to the search for more appropriate criteria and other methods such as the EPFM or non-linear fracture mechanics (NLFM). Among the concepts developed for this purpose, two have found fairly general acceptance. They are the J-integral and crack tip opening displacement (CTOD) approaches. In this chapter, only

J-integral will be considered since it is associated with the derivation of the C^* parameter which characterizes the CCG [13].

When the process zone in which damage occurs has become large enough, the K can no longer describes the stress field. Therefore, in order to find a new approach for characterizing fracture under elastic-plastic and fully plastic conditions, it seems reasonable to look for another parameter which meets the same set of conditions. For non-linear elastic material the crack tip stress field are characterized by the J-integral, which has been defined for non-linear elastic materials, which are identical to plastic material under monotonic increasing proportional loading conditions (deformation plasticity) [14].

For a cracked body the J-integral is defined along an anticlockwise contour Γ, surrounding the crack tip, the energy terms along this path (Fig. 2.5). The J-integral and then defined as follow:

$$J = \int_{\Gamma} W dy - T_i \frac{\partial u_i}{\partial x} ds \tag{2.6}$$

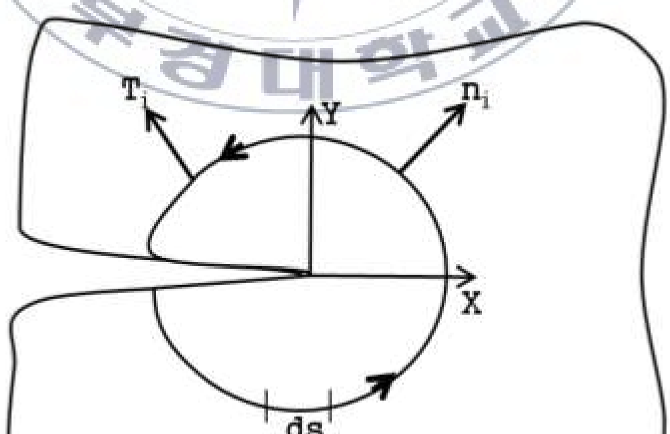

Figure 2. 5 Definition of the J contour integral surrounding the crack tip.

where W is the strain energy density of a non-linear elastic material given by:

$$W = \int_0^{\varepsilon_{ij}} \sigma_{ij} d\varepsilon_{ij} \tag{2.7}$$

and T_i is the traction vector, n_i is the outward normal to the contour Γ, and u_i is the displacement vector.

$$T_i = \sigma_{ij}\eta_j \tag{2.8}$$

It can be shown that the value of J is independent of the path Γ, which starts on the lower crack surface and ends on the upper crack surface.

Alternatively the J-integral may be obtained from the potential energy release rate of a cracked body as crack extension occurs

$$J = -\frac{\partial U}{\partial A_c} \tag{2.9}$$

where U is the potential energy (for a non-linear elastic material) and A_c is the crack area.

Under linear elastic conditions J=J_e and is related to the stress intensity factor by

$$J_e = -\frac{K^2}{E'} \tag{2.10}$$

where E' is the effective Young's modulus taken to be E under conditions of plane stress or $E/(1-v^2)$ for plane strain. For small-scale yielding conditions, the K in Eq.

(2.10) is calculated at the effective crack length a_e. In a non-linear elastic material, the J parameter may be separated into its elastic and plastic components.

$$J = J_e + J_p \tag{2.11}$$

Methods for estimating the fully plastic component of the J and Jp, are devided by three methods. These methods are the experimentally-based method (load line displacement rate), the numerical estimate: the EPRI approach, and the reference stress method. In this thesis, the method that will be used to determine the estimation of C^* and J is based on experimentally-based method (load line displacement rate). The procedures of experiment are followed the ASTM standard E-1457.

2.2.3 *J* Estimation Based on Experimentally Method

When the material can be represented as a power law or by a Ramberg-Osgood material model, then the plastic component of the J may be determined from the applied load P, and the plastic displacement Δ_p, measured at a point on the body using the general relation [22]:

$$J_p = \frac{P\Delta_p}{B_n(W-a)} H\eta \tag{2.12}$$

where B_n is the net specimen thickness between the side grooves of a specimen, W is the specimen width of half-width, and a is the crack length. The η factor in Eq. (2.12) relates J_p to an appropriate area on the load displacement record of specimen containing a crack. The parameter H is included in Eq. (2.12) to simplify the definition of η for a range geometries, and in general, the H will depend on hardening exponent N specimen geometry. The displacement of the specimen is often measured along the load line Δ^{LLD}. Alternatively the specimen crack mouth opening displacement Δ^{CMOD}, may be measured. The value H and η will be depend on whether the J is calculated using load line or crack mouth opening displacement. Solution for the η factor for a number of geometries are provided in ASTM E-1457.

2.3 Creep

Elastic and plastic strains are commonly idealized as appearing instanly upon the application of stress. Further deformation that occurs gradually with time dependent is called as creep strain. On initial loading of cracked body in an elastic-plastic material at elevated temperatures ($t = 0$), the crack tip stresses are described by the K for small scale yielding conditions or the J for significant plastic deformation. Due to the high stress generated at the crack tip, creep strains begin to accumulate in a region surrounding the crack tip, known as the creep zone.

At long times, the steady state creep conditions may be achieved, and if creep deformation can be described by a power-law, the steady state creep rate will be given by the Norton's power law according to $\dot{\varepsilon} = A.\sigma^n$. The extension of many low temperature fracture mechanics concepts into the creep regime is based on a simple analogy between the governing equations of power-law plasticity and power-law creep, and the assumption that a material deforming by the steady state creep may be described by a solution based on non-linear elasticity. Therefore, for a given load, the stress distribution in a body deforming by the steady state creep of Norton's power law equation is the same as that in a body deforming by power-law plasticity, $\dot{\varepsilon} = \sigma/E+D(\sigma/\ \sigma_{ys})^N$ (Ramberg-Osgood's equation) without the elastic term, where the creep exponent n is equal to the strain hardening exponent N.

A typical creep curve mainly consists of three distinct regions, i.e. primary creep, secondary creep, and tertiary creep, as shown in Fig. 2.6. The primary creep region is a period of decreasing creep rate during which work-hardening processes dominate and cause dislocation movements to be prevented or limited. The secondary creep region, also known as the steady state creep, usually takes the longest time of the creep process and the material creeps with a constant creep rate. The final stage of the creep process is the tertiary creep stage in which the material creeps at an increasing rate until specimens fail. For cracked bodies, for example, all the three-creep regions may be found at the same time, as shown in Fig. 2.7 [23].

2.3.1 Creep Mechanism

In polycrystalline materials, creep mechanisms are commonly divided into two main categories, dislocation creep (or known as a power-law creep) and diffusion creep. A particular creep mechanisms may predominate, for a given material, at given temperature and stress. At high temperatures, the atoms of metals are active enough to move from one position to another within metal crystals. With load applied to the material over long time, the movements of the atoms result in creep of the material. This movement, of atoms, is caused by diffusion. Vacancy diffusion occurs when an atom moves from its position to a vacancy which may be the same size as the atom itself, as shown in Fig. 2.8(a). Interstitial diffusion occurs when small atoms moves into spaces between large atoms, as shown in Fig. 2.8(b). Diffusion at grain boundaries, as shown in Fig. 2.8(c), or down cores of dislocations, as shown in Fig. 2.8(d), is much easier and may be 106 times faster than that within a crystal. This is because of the large and/or irregular atomic spacings present in these regions. At high stresses, dislocation is the dominant creep mechanism while at low stresses and high temperatures the diffusion creep is the dominant creep mechanism [24].

The creep mechanism can be summarized on a deformation map a schematic example of which is shown in Fig. 2.9, where the dominant mechanism is identified as a function of homologous stress (stress nomalized by Young's modulus) and homologous temperature (the absolute temperature T, as a function of the absolute melting temperature T_m) [25].

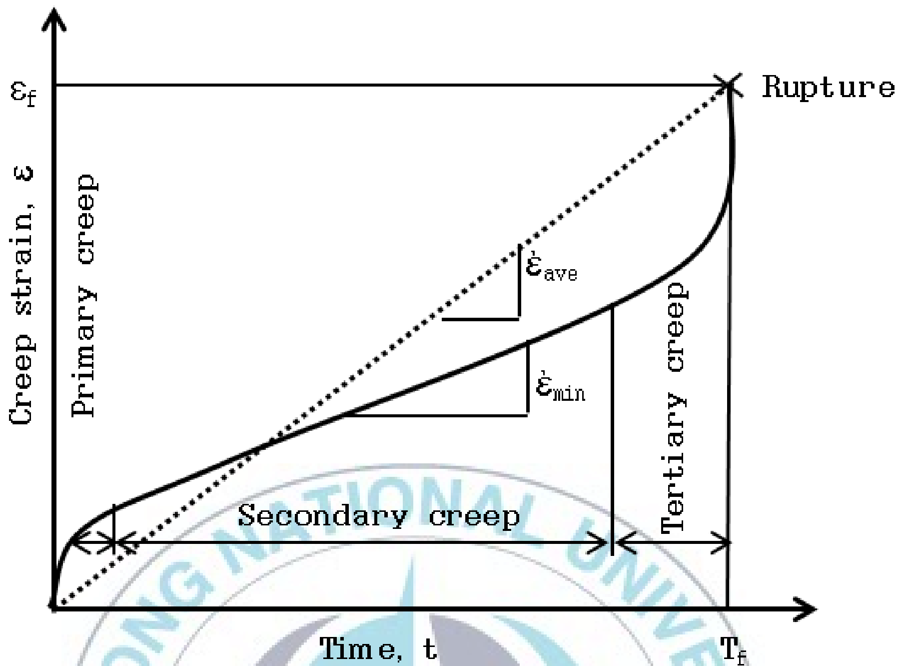

Figure 2 . 6 A typical creep strain curve.

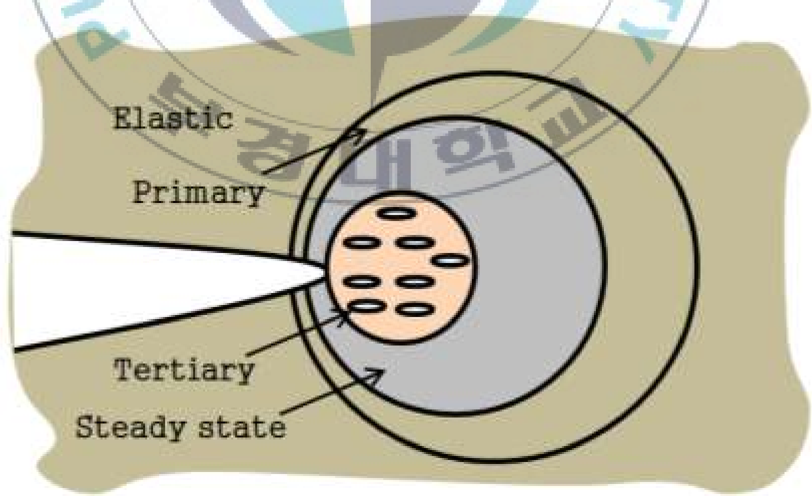

Figure 2 . 7 Creep ahead of the crack tip in a cracked body.

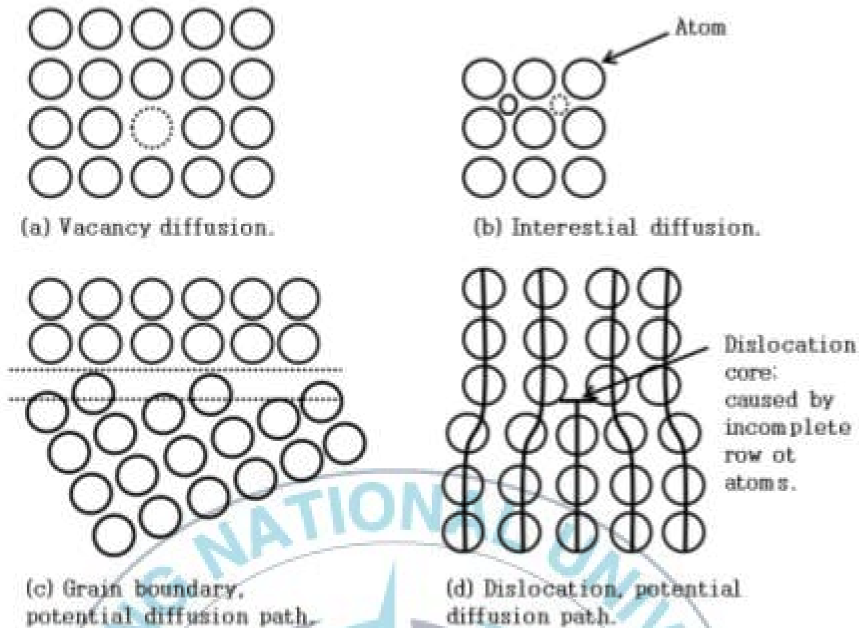

Figure 2 . 8 Creep mechanisms.

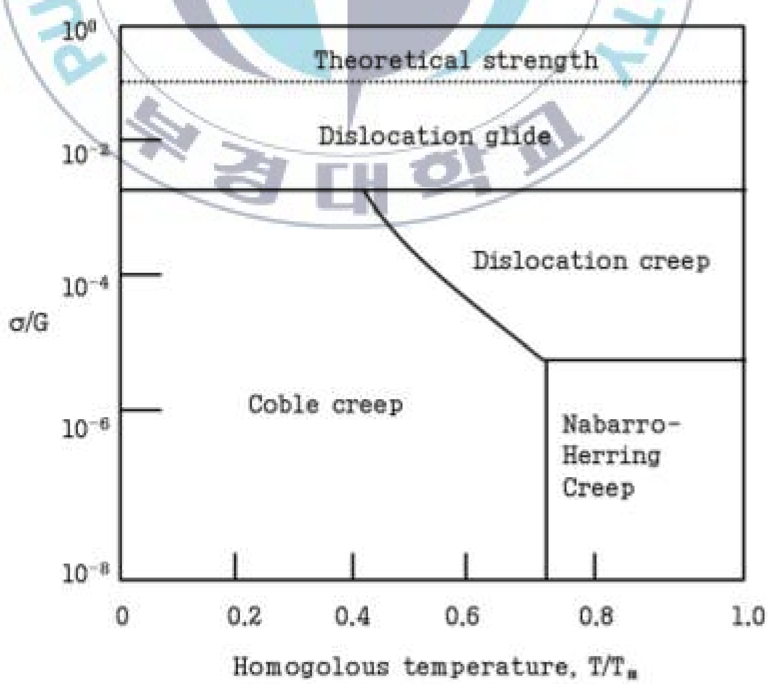

Figure 2 . 9 Schematic deformation mechanism map.

2.4 Creep Crack Growth (CCG)

2.4.1 Steady State Creep

The attainment of steady state creep conditions can be modeled as the growth of a steady state creep zone ahead of the crack tip, as shown in Fig. 2.10. Three regimes of small scale, transient and steady state creep can be distinguished for materials exhibiting elastic and power-law creep behavior. The regime exhibited at any instant depends on the size of the creep zone relative to the specimen dimensions, as shown in Fig. 2.10 [26].

If the creep zone is small in relation to the crack length and specimen dimensions, the *K* or *J* will continue to characterize the crack tip stress distribution outside the creep zone, and small scale creep conditions (SSC) are said to exist. As time proceeds, the creep zone grows, and at long times it becomes widespread. Under widespread creep conditions for a constant applied load, the steady state conditions are said to exist as the stresses become constant with time. This condition is considered as the most important in predicting of CCG of a component. Transition creep conditions describe the region between SSC and widespread creep during which the size of the creep zone is comparable to relevant dimensions. A schematic representation of these three stages of creep is given in Fig. 2.10. The SSC and transition creep conditions are characterized by time dependent crack tip stress field as the stress redistributes within the uncracked ligament.

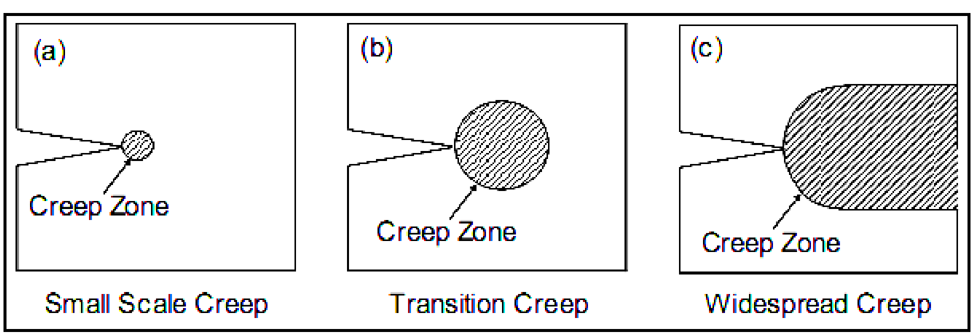

Figure 2 . 10 Schematic representation of (a) small scale (b) transition and (c) widespread creep conditions.

2.4.2 C^* Parameter

The C^* parameter is a fracture mechanics contour integral that can be used to correlate the CCG which occurs in cracked bodies under mode I loading conditions. The CCGR equation can be written by a power-law form, as follows:

$$\dot{a} = B\left(C^*\right)^q \tag{2.13}$$

where $\dot{a}$ is the creep crack growth rate, B and q are the creep constants. The creep constants B and q can be determined by plotting $log(\dot{a})$ against $log\ (C^*)$. The gradient of the plot is the q and the intercept is $log(B)$. By determining the values of B and q, it is possible to calculate CCGR at specific C^* values. Then, it is possible to predict the remaining life of cracked bodies.

By analogy with plasticity, the steady state parameter C^* has been defined separately [27]. The C^* parameter characterizes the state of stress and strain rate at a crack tip in a creeping material in the same way that *J*-integral characterizes the corresponding states of stress and strain in a plastically deforming material.

On the assumption that steady state creep deformation dominates in the ligament ahead of the crack, the definition of C^* can be defined as follows:

$$C^* = \int_{\Gamma} \left[W_s^* .\ dy - T_i \left(\frac{\partial u_i}{\partial x} \right) .ds \right] \tag{2.14}$$

where W_s^* is the strain rate energy density, which is obtained from :

$$W_s^* = \int_0^{\varepsilon_{ij}} \sigma_{ij} .d\varepsilon_{ij} \tag{2.15}$$

T_i and u_i are components of the traction and displacement rate vectors, respectively, x and y are coordinates, and ds is arc length along Γ. Clearly when secondary creep dominates for a given crack length and loading conditions, C^* will be independent of time. The integral is equivalent to the J-integral, but with strain replaced by strain rate in Eq. (2.14) and (2.15) [13]. The methods to estimate C^* almost same with the methods that are used in J-integral parameter. In this study, the experimentally-based method (load-line displacement rate) will be explained to estimate the C^* parameter.

2.4.3 C^* Estimation Based on Experimentally Method

For a power law creeping material, the C^* for a number of specimen geometries may estimate experimentally from the load and load line displacement (LLD) or crack mouth opening displacement (CMOD) rate measurements using following relations [22]:

$$C^{*LLD} = \frac{P\dot{\Delta}^{LLD}}{B_n(W-a)} H^{LLD} \eta^{LLD} \tag{2.16}$$

$$C^{*CMOD} = \frac{P\dot{\Delta}^{CMOD}}{B_n(W-a)} H^{CMOD} \eta^{CMOD} \tag{2.17}$$

Respectively, the geometry dependent functions H and η in Eq. (2.16) and (2.17) have been defined in section 2.2.3, and solutions for these functions are provided in ASTM E-1457. The superscripts LLD and CMOD are included to emphasis that these quantities are determined from the measurements of the load line or crack mouth opening displacements. The C^* value determined experimentally using Eq. (2.16) and (2.17) is here denoted C^*_{exp}.

2.4.4 Q^* Parameter

The early stage of crack growth is regarded as being important for some practical use, but when the C^* parameter is used, it has been pointed out that the characteristics of the CCGR exhibit a dual value due to nose, the precision of the estimation for CCGR improving in its early stage. It is due to the fact that the CCGR has the dependence of a different rate in the displacement rate of specimens at the early stages of crack propagation [5].

If the logarithms of experimental values of the CCGR, *log da/dt* at high temperatures is plotted against the logarithm of C^*, the experimental relation or curve reveals in many cases the dual value. In the case when the crack initiation occurs during transient creep of the region near the crack tip, i.e. $t_i < t_t$, then the relations of *da/dt* and $\dot{\delta}$ with respect to time become, respectively, as shown in Fig. 2.11(b). Therefore, the relation between *da/dt* and $\dot{\delta}$ in Fig. 2.11(c), i.e. *da/dt* and $\dot{\delta}$ shows a nose-like shape in Fig. 2.11(d) at the tail part of *da/dt* and $\dot{\delta}$. Since C^* may be represented by *da/dt* and $\dot{\delta}$ in an approximately proportional way, then in this way the relation of *log da/dt* to *log* C^* appear nose-like as in Fig. 2.11(e) for this case [5].

On the other hand, in the case when the crack initiation occurs during steady state creep of the crack tip region, as shown in Fig. 2.12(a), then the relation of *da/dt* and $\dot{\delta}$ with respect to time becomes, respectively, as shown in Fig. 2.12(b). Therefore, *log da/dt* vs *log* $\dot{\delta}$, and thus, *log da/dt* vs *log* C^* do not reveal a nose like shape, but threshold type characteristics and shown in Fig. 2.12(c) [5].

Furthermore, in the case when the crack initiation occurs during acceleration crack in the crack tip region, as shown in Fig. 2.13(a), then the relation of *da/dt* and $\dot{\delta}$ with respect to time becomes, respectively, as shown in Fig. 2.13(b). Therefore, *log da/dt* vs *log* $\dot{\delta}$, and thus, *log da/dt* vs *log* C^* do not reveal a nose-like region or threshold type characteristics, but show monotonically increasing behavior as shown in Fig.2.13(c) [5].

It was shown in Fig. 2.11 that the dual value due to nose type behavior of *da/dt* vs C^* or $\dot{\delta}$ appears when crack growth occurs during transient creep at the crack tip. Furthermore, for this case, many patterns of the nose type occur dependent on the relative value among t_t, t_i, t_s, t_a, $t_{ai.}$, where t_t = time to the termination of transient creep, t_i = time to crack initiation, t_s = time to the termination of steady state creep or starting of accelerating creep, t_a = time to the minimum crack growth rate, and t_{ai} = time to the starting of the constant rate crack growth.

A parameter for applying to the actual the CCGR must: (i) indicate the physical mechanism, which can be estimated by input conditions such as stress, temperature, and specimen shape; (ii) accurately distinguish between the variations of material properties such as activation energy, and estimate the change of characteristics represented by the acceleration of reduction of the CCGR [3].

Incidentally, the C^*-integral is dependent on creep deformation rate, which is a function of stress, temperature, specimen shape, and activation energy of deformation, etc. The differences in the CCGR characteristics caused by various conditions are controlled by the creep deformation rate. Therefore, it seems reasonable to estimate the CCGR in one band using the C^* parameter. However, it is difficult to define the changes of the CCGR characteristics due to material properties, stress, temperature, and specimen shape that prevent the application of the C^* parameter to the actual CCGR [3]. It is necessary clearly to characterize the CCGR as a function of independent variables such as material properties, stress, temperature, and specimen shape.

In order to apply these characteristics, Yokobori et al. has proposed the Q^* parameter. The Q^* parameter was defined as the exponent of the exponential in the thermal activation process equation. Their experiments resulted that the Q^* parameter could reasonably evaluate the CCGR by a simple monotical linear function without a dual value due to nose on the early stage of CCG curve and it was regarded as an independent parameter that could distinguish between the variation of material properties [3].

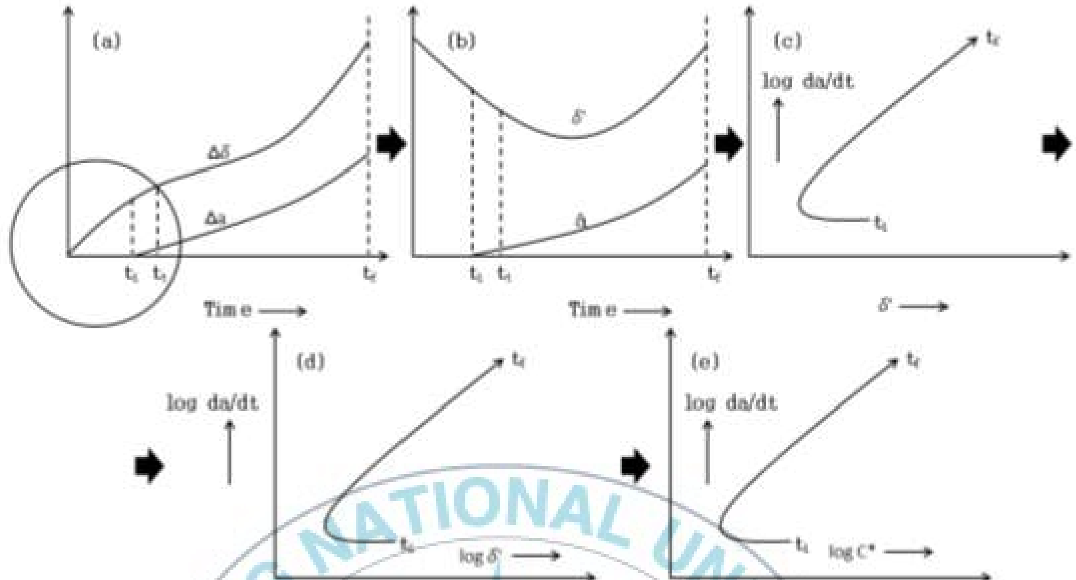

Figure 2 . 11 Schematic illustration of evaluating method by *log da/dt* vs *log* $\dot{\delta}$ projection t_i < $t_{t.}$ [5].

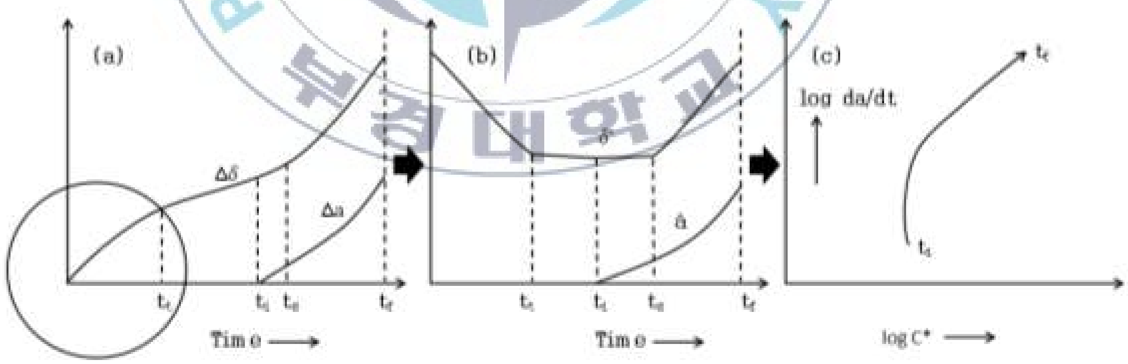

Figure 2 . 12 Schematic illustration of evaluating method by *log da/dt* vs *log* $\dot{\delta}$ projection t_t < t_i< $t_{s.}$ [5].

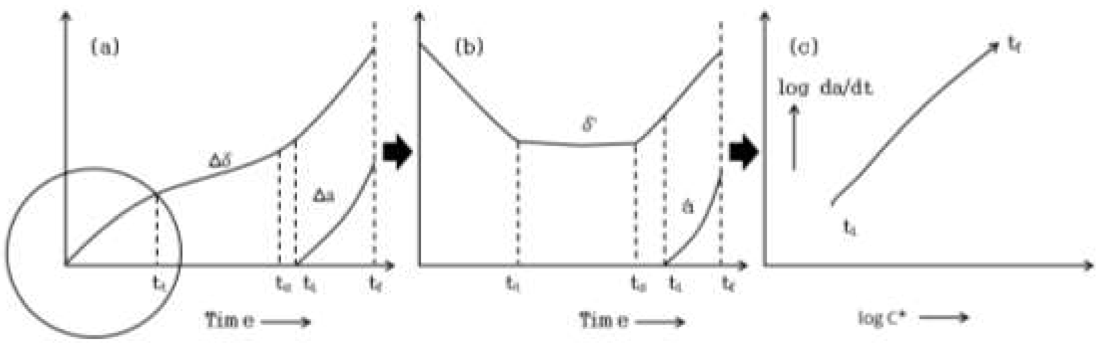

Figure 2 . 13 Schematic illustration of evaluating method by *log da/dt* vs *log* $\dot{\delta}$ projection t_s < $t_{i.}$ [5].

Fig. 2.14 shows an estimation of the test result for an outer compact tension specimens by using the Q^* parameter. From this figure, it is obvious that the CCG is accelerated by an acceleration of creep deformation rate. For various conditions of temperature or stress, this parameter can distinguish the difference in the CCGR caused by the variation of material changes by parallel movement along the horizontal axis within the bandwith of one order of magnitude, which is the general precision provided by estimation with the C^* parameter [3].

Fig. 2.15 shows the crack growth rate estimated by the C^* parameter. Such level of material variation can not be distinguished by the estimation of the C^* parameter, which is involved in the same band.

Fig. 2.16 shows the crack growth rate estimated by the C^* parameter for SUS 304 stainless steel and CrMoV steel. Apparent differences can not observed between the CCGR of CrMoV steel that of SUS 304 stainless steel, so the C^* can not be used to distinguish creep crack growth chracteristics for various materials [3].

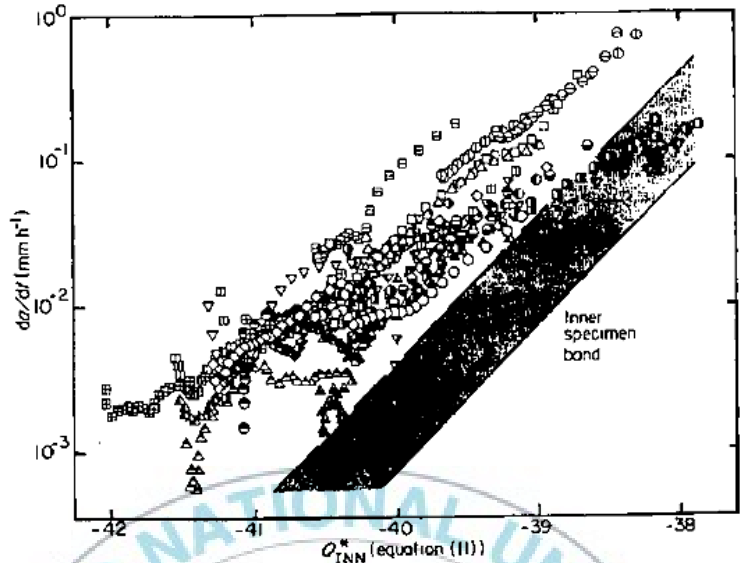

Figure 2 . 14 Comparison of the CCGR characteriscs between inner and outer parts of turbine rotor as estimated by the Q^*_{INN} parameter [3].

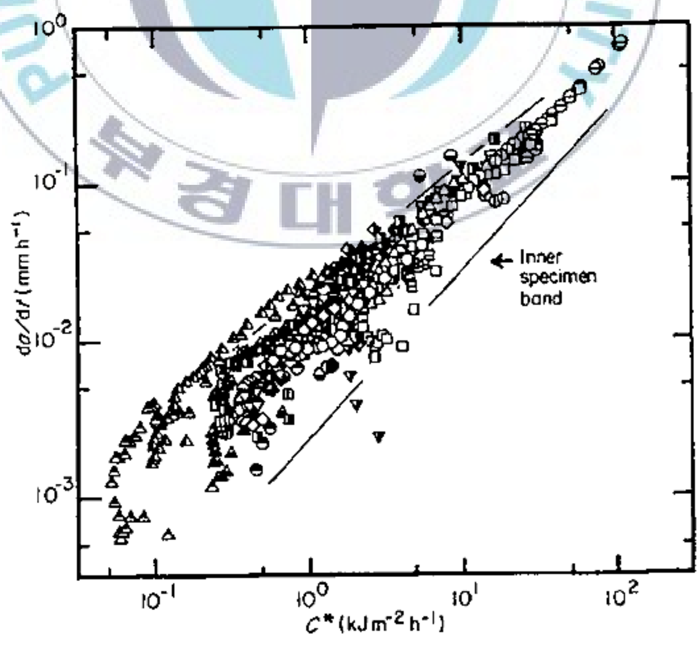

Figure 2 . 15 The CCGR estimated by the C^* parameter (CrMoV CT specimen) [3].

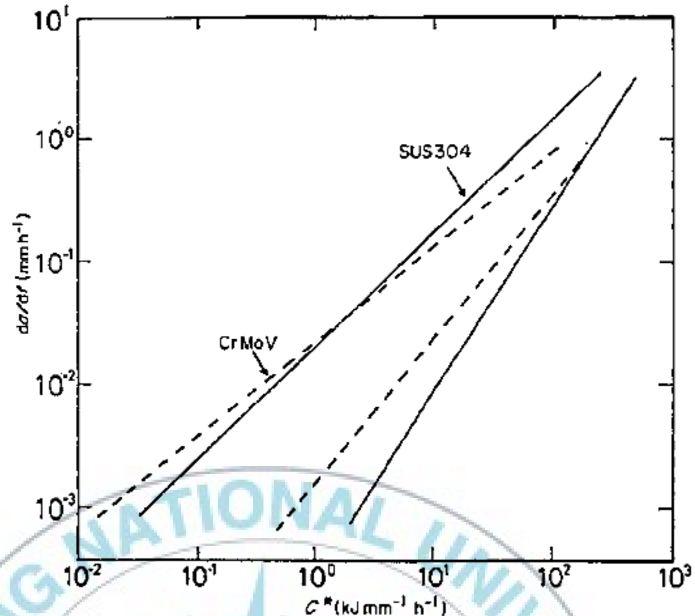

Figure 2 . 16 Comparison of characteristics of the CCGR between CrMoV steel and SUS 304 steel as estimated by the C^* parameter [3].

2.4.5 Q^* Estimation Based on Activation Energy

Activation energy is the minimum energy barrier that must be met for a chemical reaction to happen or treshold energy that one state must acquire before reaching transition state. The description of activation energy can be seen in Fig. 2.17.

In Fig. 2.17, the force must be applied with an amount of minimum energy to pass the rock from the peak of the hill (transition state). In this case, the minimum energy that is needed to pass the peak of the hill is termed as activation energy. A condition with a large activation energy requires much more energy to reach transition state and vice versa. Creep occurs when a metal is subjected to a constant tensile load at an elevated temperature (undergo a time-dependent increase in length). Since material have its own different melting point, each will creep when the homologous temperature (T_h) > 0.5.

$$Homo\log ous\ temperature(T_h) = \frac{Testing\ temperature(T_t)}{Melting\ temperature(T_m)} > 0.5 \tag{2.18}$$

On that condition (homologous temperature), the atoms in material will move faster and some phenomena occur such diffusion process, greater mobility of dislocation (climb), and increased amount of vacancies.

The Q^* parameter has been originally proposed by Yokobori et al. for correlating or characterizing the CCGR [3]. The CCGR has been expressed in term of an activation process equation, and the Q^* parameter was defined as the exponent of the exponential in the thermal activation process equation for *da/dt*, in which the activation energy is expressed in terms of free energy, as follows [3]:

$$\frac{da}{dt} = A^* \exp\left(-\frac{U}{RT}\right) \tag{2.19}$$

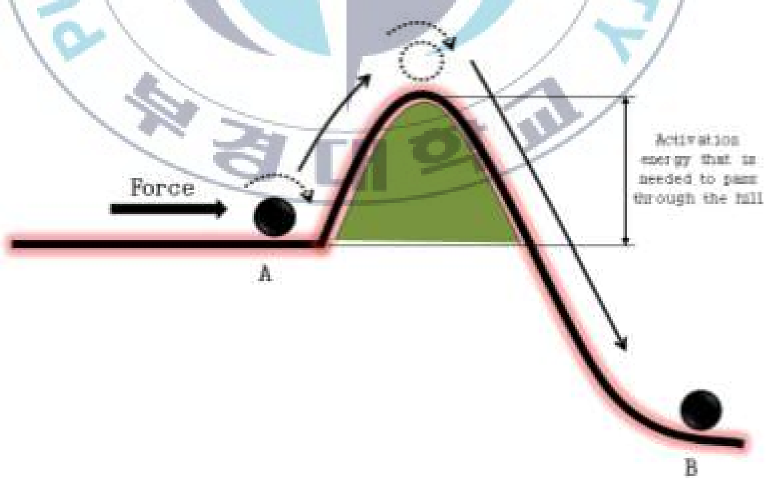

Figure 2 . 17 Ilustration of the activation energy.

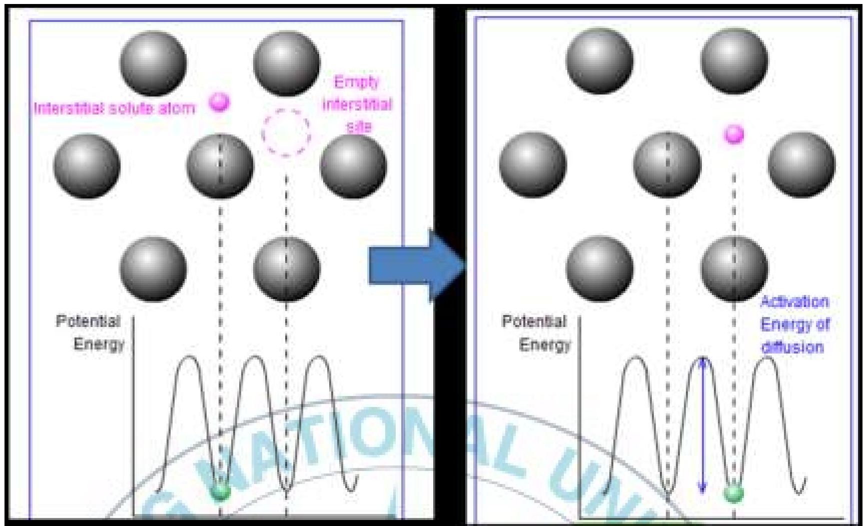

Figure 2 . 18 Interestial diffusion.

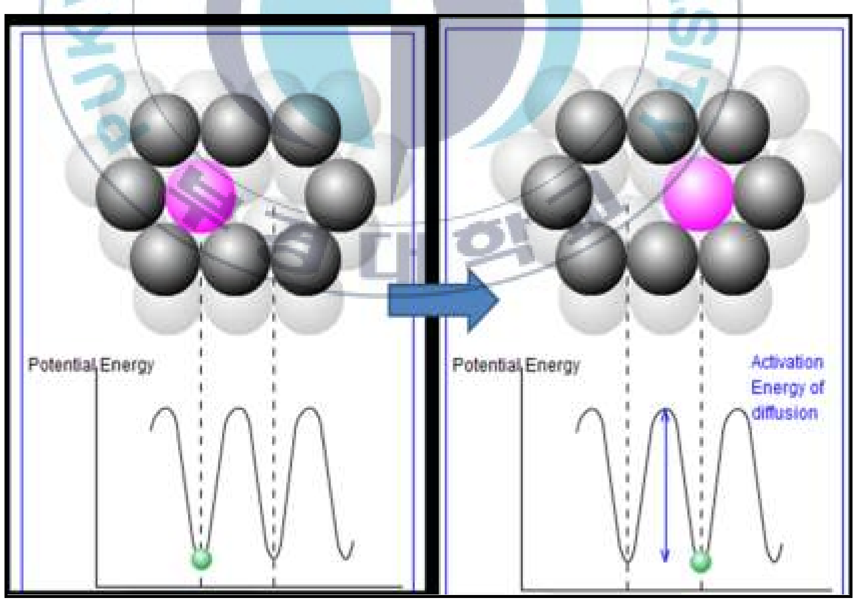

Figure 2 . 19 Substitutional diffusion.

The equation above is based on Arrhenius's equation. Arrhenius performed experiments that correlated chemical reaction rate constants with temperature. As temperature increase, gas molecul velocity (diffusion) also increase. Kinetic energy of molecules is directly proportional to the velocity of the molecules. So when the temperature increases, kinetic energy also increases. This means that as temperature increases, more molecules will have higher kinetic energy, thus the fraction of molecules that have high enough kinetic energy to exceed the minimum energy needed for a reaction also increase. The fraction of molecules that has an energy equal to or greater than activation energy is given by the exponential term.

The exponential term in Arrhenius's equation implies that the rate constant of a reaction increases exponentially when the activation energy decrease. Since the rate of reaction is directly proportional to the rate constant of a reaction, the rate increases exponentially as well. Because a reaction with a small activation energy does not require much energy to reach the transition state, it should proceed faster than a reaction with a larger activation energy.

III. Experimental Method

3.1 Experimental Procedures

To characterize the CCGR of modified 9Cr-1Mo steel, a series of creep and CCG tests was performed at Korea Atomic Energy Research Institute (KAERI). The 1/2 inch CT specimens were used. The creep and CCG tests were carried out under various applied load levels at 550^{o}C and 600^{o}C. The LLD data were acquired through PC with real time variations during the CCG tests, and crack lengths were monitored using the direct current potential drop (DCPD) technique. The LLD rates and the corresponding crack lengths were then used to calculate the K and C^* parameter, i.e, the fracture mechanics parameters used to correlate CCGR of cracks in cracked specimens. These data were used to obtain the activation energy to calculate the Q^* parameter.

3.2 Material Composition

The modified 9Cr-1Mo steel used in this study was a hot rolled plate of 16 mm in thickness. The conditions of heat treatment condition were normalized and tempered at 1015 ^{o}C/1min/mm and 770 ^{o}C/3min/mm, respetively [2]. The chemical composition is given in Table 3.1.

Table 3 . 1 Chemical composition of modified 9Cr-1Mo steel (wt. %).

C	Si	Mn	P	S	Ni	Cr	Mo	Cu	V	Al	N	Nb
0.115	0.23	0.415	0.012	0.0014	0.22	8.9	0.869	0.038	0.194	0.020	0.0513	0.073

3.3 Specimens Preparation

The CT specimens had a width (W) of 25.4 mm, a thickness (B) of 12.7 mm and side grooves with 10% depth, as shown in Fig. 3.1 and 3.2. The initial crack ratio (a/W) was about 0.5.

The creep test specimens were machined to a cylindrical shape with a 30 mm gauge length and 6 mm diameter. All the specimens were taken along the rolling direction. The gauge section of the creep specimens was polished using #1000-grit sand papers and stroking along the specimen axis.

3.4 Creep Tests

The creep tests were conducted according to the ASTM standard E-139 [28]. All tests were performed using dead weight lever arm machines with a lever arm ratio of 20:1. To heat-up and keep the specimens at constant temperature, a three-zone electrical resistance furnace was used. The temperature was monitored and controlled to vary no more than ± 2^{o}C at the test temperatures. To measure the specimen temperature, a “K-type” thermocouple was attached on the gauge length of the specimens. Constant-load creep tests were carried out under various load at 550^{o}C and 600^{o}C.

To measure the axial displacement, a high-precison extensometer was attached to ridge on the specimen. The extensometer and pull rods were manufactured from a high temperature creep resistance alloy (Inconel 718) to avoid any aditional creep strain contribution from these components in the measured displacement. To record the displacement a linear variable differential tranducer (LVDT), which was previously calibrated, was mounted at the ends of the extensometer outside the furnace. The output voltage from the LVDT was converted into a displacement by calibrating the LVDT with a specially mounted micrometer. The calibration of LVDT was done before each test to ensure linearity.

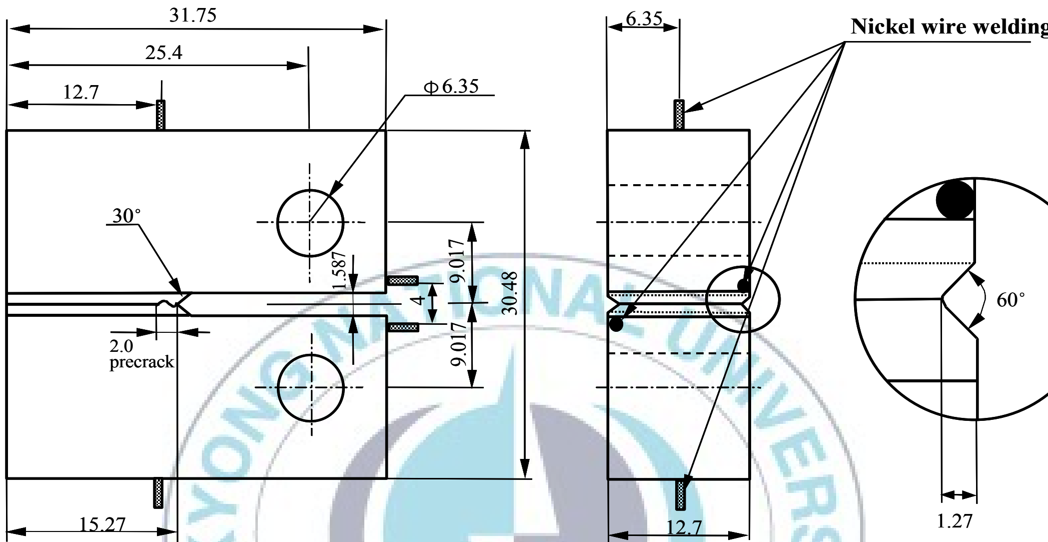

Figure 3. 1 Dimensions of ½ CT specimen.

Figure 3 . 2 Shape of the CT specimen with the side grooves.

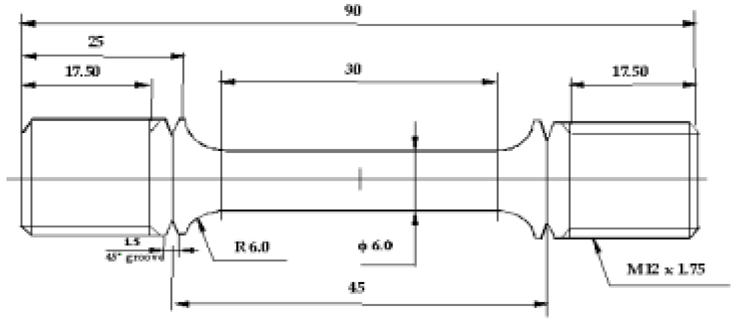

Figure 3 . 3 Dimensions of the creep specimen.

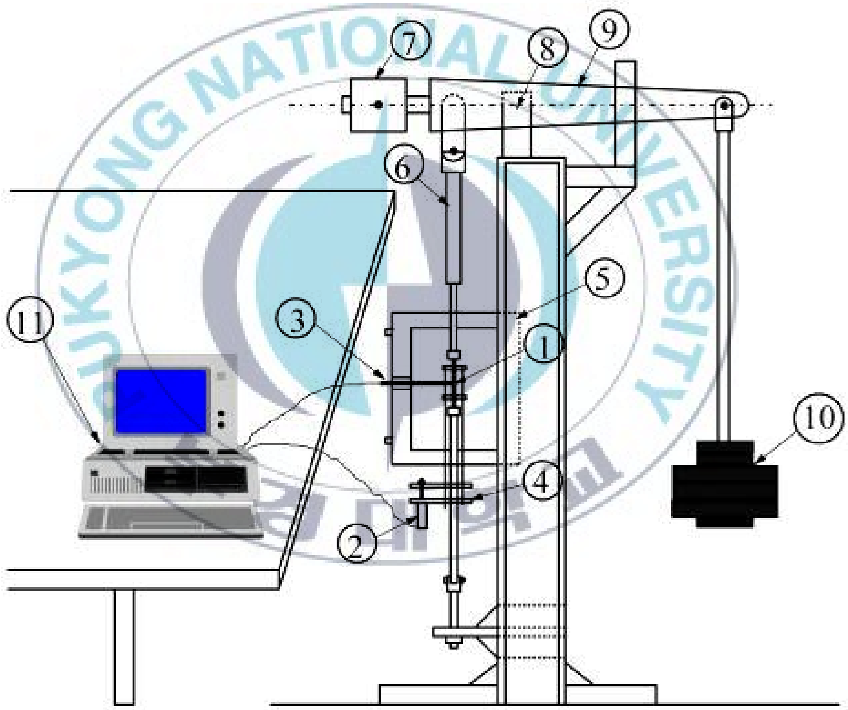

1. Creep specimen
2. Linear gage
3. Thermocouple
4. Extension
5. Furnace
6. Pull rod
7. Balance weight
8. Support
9. Arm
10. Weight
11.Personal computer

Figure 3 . 4 Appratus of creep test machine.

When the test had been set-up completely, a small fraction of the test force (±10% of application load) was applied before and during heating of the specimen. This usually improves the axiality of force application by reducing the displacement of the specimen and load rods due to lateral forces from furnace packing and thermocouple wires. After that, the furnace was switched on. However, prior to the loading, a period of at least 60 minutes was allowed to enable the apparatus to reach and stabilize at a target temperature. The temperature and displacement were continously acquired by a data logger. Temperature recording was started before applying the load to obtain the initial displacement. The loading procedure took between 2 ~ 3 minutes to avoid any unnecessary shock [28]. The steady state creep rate was obtained by calculating the experimental creep curves.

3.5 Creep Crack Growth Tests

The CCG tests were carried under various applied load levels at 550^{o}C and 600^{o}C, as shown in Table. 3.2 and 3.3. Where a_0 is the pre-cracked, a_{pf} is the predicted final crack size that was determined from Johnson's formula, a_{mf} is the measured final crack size that was determined from nine points method, B_N is the net thickness, B is the thickness of CT specimen, and the last column is the validation of the measurement. All the CCG tests were conducted according to the standard procedure of ASTM standard E-1457.

For the same reason as for the creep tests, all the CCG tests were conducted using dead weight lever arm machines with a lever arm ratio of 20:1. The procedure to set-up the CCG tests was similar to the one used for the creep tests.

The DCPD technique has been used for many decades as method of monitoring crack initiaion and growth in controlled laboratory tests. In fact, this method has gained wide acceptance in fracture research as one of the most accurate and efficient methods for monitoring the initiation and propagation of cracks. The proof of its success is its popularity in the field of fatigue crack growth testing [29-31], and by its accepetance in ASTM standard E-1457 for resolving crack extension of at least 0.1 mm. This technique was used to measure the growing crack length for all CCG tests herein.

The DCPD technique relies on the fact that there will be disturbance in the electrical potential field about any discontinuity in a current-carrying body, where the magnitude of disturbance will depend directly on the size and shape of the discontinuity [29]. The method involves passing constant current through a cracked test specimen and measuring the change in electrical potential across the crack plane as the crack propagates. As the crack propagates, the uncracked cross-sectional area of the test piece decreases which lead to an increase of its electrical resistance and as a result, the potential difference between two points spanning the crack rises. The DCPD is continually recorded on a chart and data logger and the crack length is calculated by using an appropriate calibration curve.

The constant current flowing through the specimen can be either an alternating current (A.C.) or a direct current (D.C.) source. Each of these methods has its advantages and disadvantages. For A.C., the current density in non-uniform through the thickness of the specimen. The current flow is also affected by the magnetic field it engenders, producing a higher current density occuring near the surface of the specimen. This effect, so-called ‘skin effect’, is more pronounced at high frequencies and in materials of high magnetic permeability. Thus, at high frequencies where the ‘skin effect’ becomes pronounced, the A.C. method will be more sensitive to crack length changes near the surfaces of the specimen. Consequently, this method may not be suitable if through the thickness crack front curvature is significant or extra care must be taken when used. However the ‘skin effect’ may be lessened by using lower A.C. frequencies. On the other hand, for D.C. method, the current density is uniform throughout the thickness of the specimen. The fact that the supply current flows throughout the specimen imply a higher current than the A.C. method is required. This puts severe constraints on the supply electronics, providing high amperage of continous and constant current is not simple. At equal potential levels the A.C. system provides much greater sensitivity and better precision, while still operating at lower current level [30].

A schematic illustration of the CCG testing apparatus is shown in Fig. 3.5. The CCG tests were carried out at constant load. The load-line deflection was measured by linear gauge assembly attached to the specimen and crack length was determined by DCPD method. The crack extension data were continuously collected using a data acquisiton system. A “K-type” thermocouple was attached under 2 ~ 5 mm from the precracking position of the CT specimen. The temperature was controlled within ± 2°C during the tests. A current of 8 A was applied. The output voltage was recorded by PC and converted to crack length by using Johnson’s formula as follows [32]:

$$a = \frac{2W}{\pi}\cos^{-1}\frac{\cosh(\pi y_0/2W)}{\cos v/v_0\left[\cosh^{-1}\{(\cosh(\pi y_0/2W)/\cos(\pi a_0/2W))\}\right]} \tag{3.1}$$

where a is the crack length, a_o is the initial crack length, V is the output voltage, V_o is the initial output voltage, W is the specimen width, and y_o is a half distance between output potential leads. After the CCG tests, the CT specimens were cooled down in a liquid nitrogen solution and fractured to measure the final crack length.

The position of ledwire connections for CT specimen was chosen according to ASTM standard E-1457 and shown in Fig. 3.6.

Table 3 . 2 The CCG test conditions and crack size measurements at 550^{o}C**.**

Sp.	Load (N)	a_0(mm)	a_{pf}(mm)	a_{mf}(mm)	B_N(mm)	B(mm)	$0.85 \leq (a_{pf}-a_0)/(a_{mf}-a_0) \leq 1.15$
G91-6	6200	12.602	15.815	15.828	10.093	12.625	0,99597
G91-7	6500	12.665	18.193	18.088	10.096	12.603	1,019362
G91-8	6800	12.632	14.692	14.661	10.109	12.638	1,015278
G91-9	6000	12.665	15.087	15.037	10.074	12.615	1,021079
G91-10	7000	12.590	14.272	14.164	10.132	12.640	1,068615
G91-12	6800	12.760	14.229	14.332	10.099	12.594	0,934478
G91-13	6800	12.698	14.268	14.263	10.103	12.626	1,003195

Table 3 . 3 The CCG test conditions and crack size measurements at 600^{o}C.

Sp.	Load (N)	a_0(mm)	a_{pf}(mm)	a_{mf}(mm)	B_N(mm)	B(mm)	$0.85 \leq (a_{pf}-a_0)/(a_{mf}-a_0) \leq 1.15$
G91-1	3800	11.604	14.670	14.928	10.014	12.672	0,922383
G91-3	4500	11.538	13.912	14.105	10.104	12.632	0,924815
G91-4	5000	11.669	13.086	13.283	10.119	12.654	0,877943
G91-7	4000	11.428	13.812	14.351	10.106	12.677	0,8156
G91-8	5000	11.456	13.624	13.694	10.161	12.688	0,968722
G91-9	5000	11.378	13.690	13.726	10.168	12.655	0,984668
G91-12	4800	11.634	17.401	17.620	10.159	12.648	0,963415
G91-13	5200	11.590	17.153	17.098	10.195	12.668	1,009985
G91-15	4000	11.673	14.785	14.179	10.165	12.676	1,24182
G91-16	5000	11.614	14.224	14.355	10.179	12.68	0,952207
G91-17	5000	11.605	13.436	13.283	10.172	12.67	1,09118
G91-18	6000	12.686	25.002	24.529	10.174	12.664	1,039939

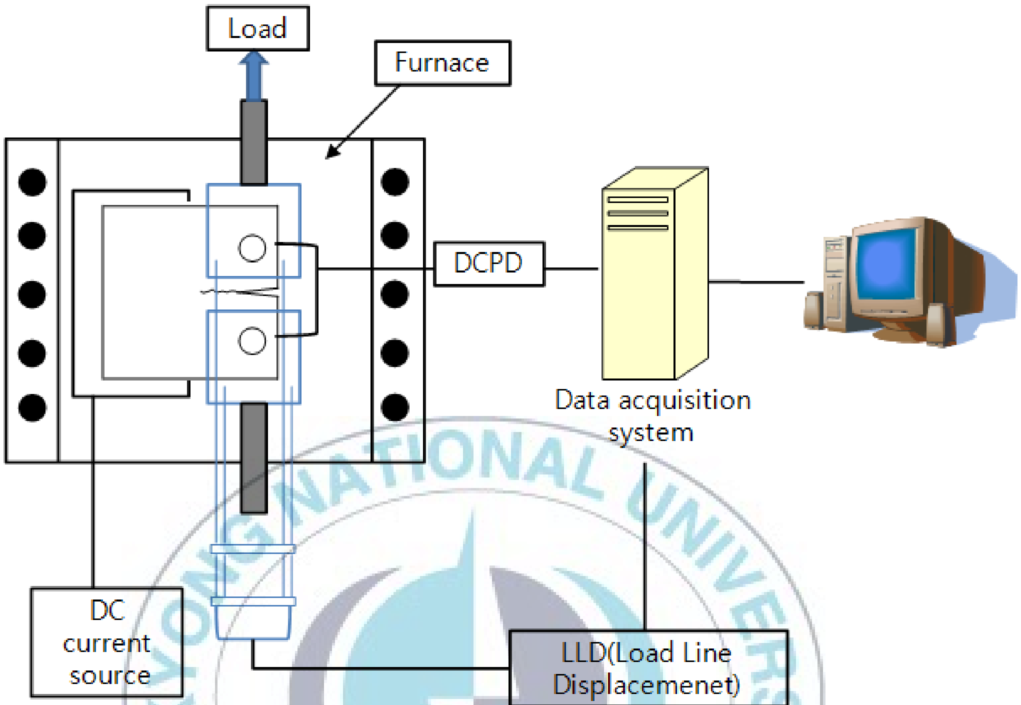

Figure 3 . 5 A schematic illustration of CCG testing apparatus.

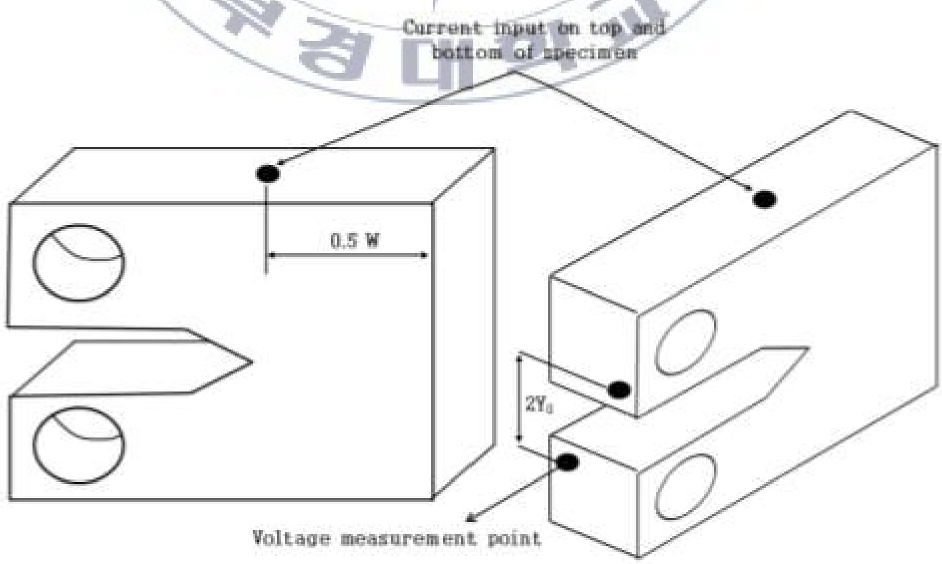

Figure 3 . 6 Lead position for measuring potential drop in CT specimen.

3.6 Determination of CCGR Based on Load Line Displacement

The determination of the CCGR is devided into two categories of determination based on load line displacement and determination based on activation energy. On the next chapter, the results are given and compared between the two methods.

Validity criteria are specified in ASTM standard E-1457 for the use of fracture mechanics parameters. Firstly, the C^* parameter is suitable for characterizing crack growth in creep-ductile metals in which the crack growth is accompanied by substantial amounts of the creep deformation and the effects due to crack growth can be neglected. Conversly, the K is more suitable for characterizing steady-state CCG in creep-britle materials in which the crack tip and creep zone boundary move at the same rate. To identify the valid regions for the C^* and K, the ratio of load line displacement rate between creep part and total load line displacement rate must be determined first (Δ^C/Δ^{exp}). If $\Delta^C / \Delta^{Exp} \geq 0.5$, the data are classified as being creep-ductile, and the candidate crack growth rate relating parameter C^* is recomended. If $\Delta^C/\Delta^{Exp} \leq 0.25$, the data are classified as being creep-britle, and then the candidate parameter K is used [32].

Secondly, the transition time t_T must be exceeded. It is to ensure the crack extension is occuring under extensive creep conditions. In order to verify this assumption, the t_T from small scale to extensive creep using Eq. (3.2) must be calculated for each point and the largest value of t_T is defined as the transition time [25].

$$t_T = \frac{K^2\left(1-v^2\right)}{E\left(n+1\right).C*_t} \tag{3.2}$$

$$K = \frac{P}{B^{1/2}B_N^{1/2}W^{1/2}}\left[\frac{2+a/W}{\left(1-a/W\right)^{3/2}}\right]f\left(a/W\right) \tag{3.3}$$

$$f\left(a/W\right) = 0.886 + 4.64\,a/W - 13.32\left(a/W\right)^2 + 14.72\left(a/W\right)^3 - 5.6\left(a/W\right)^4$$

The magnitude of C^*_t can be estimated, as follows:

$$C_t^* = \frac{P\dot{\Delta}^C}{\sqrt{BB_N}W} F'/F \tag{3.4}$$

$$F'/F = \left[\frac{1}{2+a/W} + \frac{3}{2(1-a/W)}\right] + \frac{f'}{f} \tag{3.5}$$

$$f = 4.64 - 26.64(a/W) + 44.16(a/W)^2 - 22.43(a/W)^3$$

In chapter 2, section 2.4.3, it was shown that the creep fracture parameter C^* can be calculated experimentally from the load line displacement rate for extension at a constant load. However, to determine the C^* according to Eq. (3.6), it is necessary to determine the creep displacement rate, $\dot{\Delta}^C$.

$$C^{*LLD} = \frac{P\dot{\Delta}^C}{B_n(W-a)} H^{LLD} \eta^{LLD} \tag{3.6}$$

During any particular specimen tests, only the total experimental load-line displacement rate $\dot{\Delta}^{Exp}$ can be measured. The experimental displacement rate can be separated into three components as shown in Eq. (3.7) [17].

$$\dot{\Delta}^{Exp} = \dot{\Delta}^{pl} + \dot{\Delta}^{el} + \dot{\Delta}^C \tag{3.7}$$

The first component is a plastic contribution, which was considered as negligible. The second is an elastic contribution $\dot{\Delta}^{el}$, due to the changing crack length so that Eq. (3.8) may be written as:

$$\dot{\Delta}^{Exp} = \dot{\Delta}^{el} + \dot{\Delta}^C \tag{3.8}$$

On the above basis, the total load-line displacement rate $\dot{\Delta}^{Exp}$ can be partitioned into a instantaneous (elastic) part $\dot{\Delta}^{el}$ and a time dependent part that is directly associated with the accumulation of creep strains $\dot{\Delta}^{C}$ using [32]:

$$\dot{\Delta}^{el} = \frac{\dot{a}B}{P}\left[\frac{2K^2}{E'}\right] \tag{3.9}$$

where $\dot{a}$ is the crack growth rate, P is the applied force, B is the specimen thickness, K is the stress intensity factor, and E' is the effective elastic modulus ($E/1\text{-}v^2$) for the plane strain and E for the plane stress.

In the presence of significant plastic deformation, the deflection rate due to creep can be estimated using the following equations [32]:

$$\dot{\Delta}^{c} = \dot{\Delta} - \frac{\dot{a}B_N}{P}\left[\frac{2K^2}{E'} + (m+1)J_p\right] \tag{3.10}$$

where J_p is the fully-plastic contributions to J-integral and m is the stress exponent in the Ramberg-Osgood stress versus strain relationship [32].

$$J_p = \frac{D_1 h_1(a/W, m)}{\left(\sigma_{ys}(W-a)\right)^m}\left(\frac{P}{1.455 B_N \alpha}\right)^{m+1} \tag{3.11}$$

where $\alpha = (\varphi^2+2\varphi+2)^{1/2}-(\varphi+1)$, and $\varphi = 2a/(W-a)$. D_1 and m are the constants that related to the material stress-strain behavior and h_1 is a function of a/W and m and is given in Table in ASTM standard E-1457.

3.7 Determination of CCGR Based on Activation Energy

The CT specimens were tested at a specific value of stress (isostress) and at a specific value of temperature (isothermal). At a specific value of stress, the relation between absolut temperature T and CCGR da/dt, which were characterized by the K parameter, indicates an Arrhenius-type temperature dependence; i.e. with an increase in K-value, the absolute value of the gradient decreases, as shown in Fig. 3.7. The figure shows that the following equation of Arrhenius type holds [3]:

$$\frac{da}{dt} = A * \exp\left(-\frac{U}{RT}\right) \tag{3.12}$$

The line gradients shown in Fig. 3.7 correspond to activation energy. These gradients decrease with an increase of the K. Therefore, the value of activation energy U was obtained from the tangent value of the straight line. The activation energy can be represented by a function of the K parameter as shown in Fig. 3.8:

$$U = \Delta f_1 - \Delta f_2 \ln(K) \tag{3.13}$$

The value of Δf_1 is approximately equal to the activation energy of self-diffusion which is the spontaneous movement of atom to a new site in a crystal of the same type. Moreover, the plot of creep exponent n, versus the inverse absolute temperature $1/T$, indicates a linearly increasing function, as shown in Fig. 3.9.

At a specific value of stress as shown in Fig. 3.10, the following relation can be expressed as:

$$K = A\sigma^B \tag{3.14}$$

Furthermore, at the isothermal and isostress conditions, the following relation was proved experimentally to be expressed as [3]:

$$\frac{da}{dt} = A(\sigma_g, T)K^{-n} \tag{3.15}$$

The σ_g was obtained by substituting zero for the crack length a into the following equation [3]:

$$\sigma_{net} = \frac{P}{(BB_N)^{1/2}(W-a)}\left\{1+\frac{3(W+a)}{(W-a)}\right\} \tag{3.16}$$

Based on Eqs. (3.12) ~ (3.16) and further analysis of the experimental data by the similiar procedure, Yokobori et al. determined the crack growth rate formulation based on the activation energy. It can be expressed in terms of isothermal and isostress conditions, as follows [6-8]:

$$\frac{da}{dt} = A'(\sigma_g, K)\exp\left(-\frac{U}{RT}\right) \tag{3.17}$$

Using Eq. (3.17), the Q^* parameter was obtained. The Q^* parameter is defined as the exponent of the exponential function in the thermal activation process equation. Therefore, the part of the last bracket in Eq. (3.17) corresponds to the Q^* parameter, as follows:

$$\frac{da}{dt} = A^*\exp(Q^*) \tag{3.18}$$

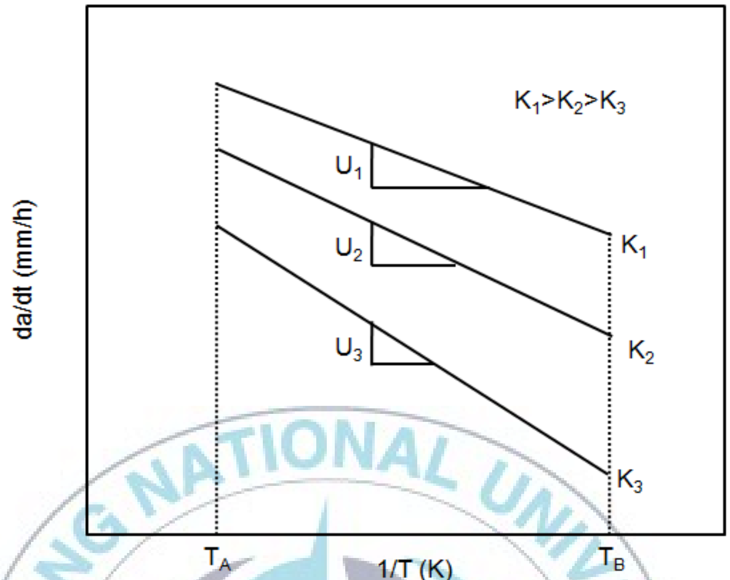

Figure 3 . 7 Schematic illustration for Arrhenius-type relation [3].

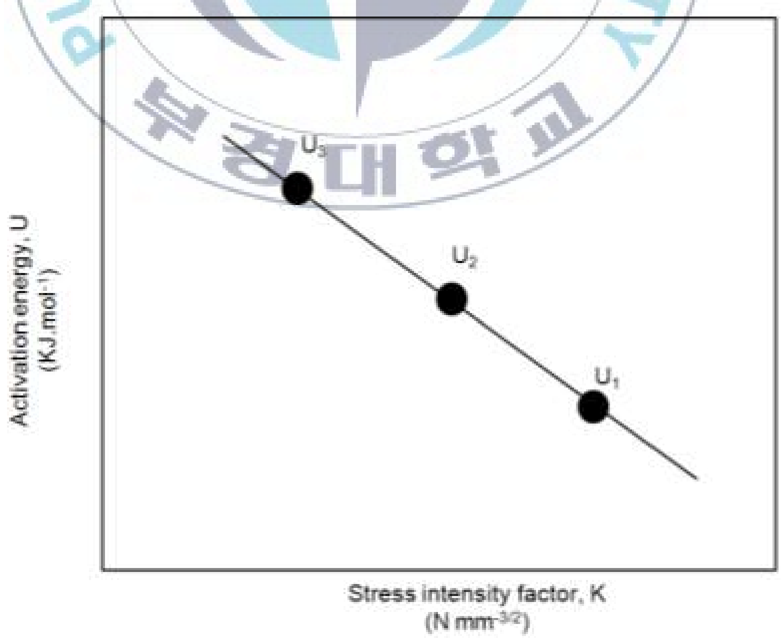

Figure 3 . 8 Schematic relationship between activation energy and *K* [3].

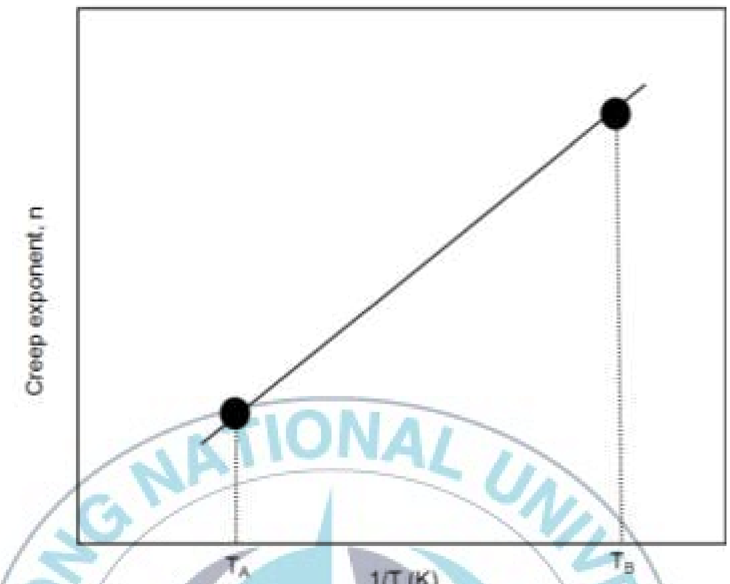

Figure 3 . 9 Schematic relationship between *n* and absolute temperature [3].

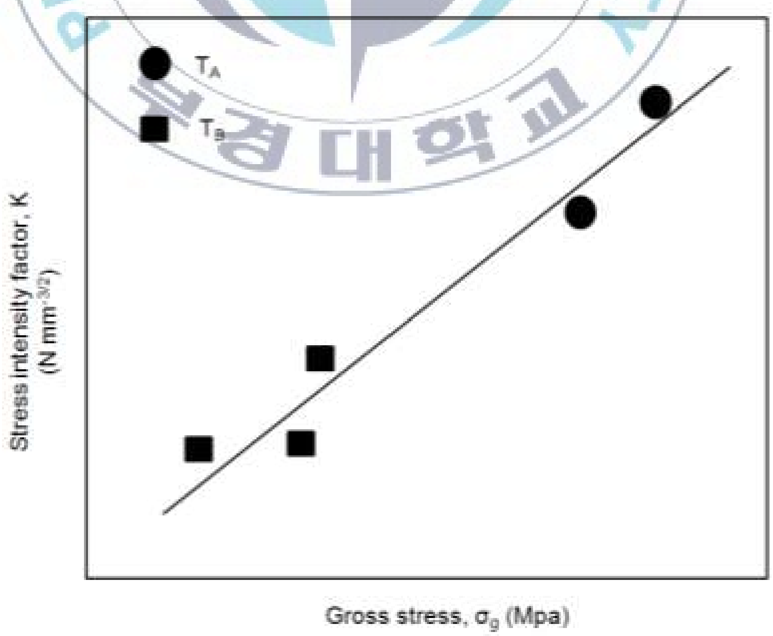

Figure 3 . 10 Schematic relationship between gross stress and *K* [3].

IV. Results and Discussion

4.1 Creep Test Results

To obtain material properties of the modified 9Cr-1Mo steel, the tension tests were conducted at 550°C and 600°C, and also creep tests were conducted under various applied load levels at the identical temperature of 550°C and 600°C. Tension tests were conducted with 1mm/min of cross head speed using displacement control methods. Displacement was measured by attaching high-temperature extensometer of 25.4 mm on gauge section of the specimens. The plastic constants *D* and *N* from the tension tests were calculated using Ramberg-Osgood's equation.

$$\dot{\varepsilon}_p = \frac{\sigma}{E} + D\left(\frac{\sigma}{\sigma_{ys}}\right)^N \tag{4.1}$$

where the first term on the right side, σ/E is equal to the elastic part of the strain, and the second term, $D(\sigma/\sigma_{ys})^N$ accounts for the plastic part. The parameter of *D* and *N* describes the hardening behavior of the material. The obtained material properties are listed in Table 4.1.

From the creep tests, the creep constants of *A* and *n* were obtained using Norton's law equation.

$$\dot{\varepsilon}_{ss} = A(\sigma)^n \tag{4.2}$$

Table 4.2 shows the results obtained a series of creep tests under the stress levels of 180 MPa ~ 300 MPa at 550°C. Table 4.3 shows the creep test results conducted under the stress levels of 120 MPa ~ 180 MPa at 600°C. The creep rate data can be used to determine the creep constants *A* and *n*. These constants were determined by the logarithmic graph, as shown in Fig. 4.1 and 4.2.

Table 4 . 1 Mechanical properties of modified 9Cr-1Mo steel under various loads at 550°C and 600°C.

Temp (°C)	E (GPa)	σ_{ys} (MPa)	Plastic constants $\dot{\varepsilon}_p = D(\sigma/\sigma_{ys})^N$		Creep constants $\dot{\varepsilon}_{ss} = A\sigma^n$	
			D	N	A (MPa^{-n}/h)	n
550	175	340	0.00123	15.45	1.29E-37	13.70
600	164	247.5	0.0017	6.4	1.28E-27	9.98

Table 4 . 2 Creep rate results at 550°C.

Applied stress (MPa)	Creep rate (1/h)
180	1.10E-6
200	1.10E-6
220	2.19E-5
220	2.19E-5
230	2.91E-5
240	4.05E-5
240	3.96E-5
250	6.10E-5
260	1.28E-4
280	4.81E-4
300	1.67E-3

Table 4 . 3 Creep rate results at 600°C.

Applied stress (MPa)	Creep rate (1/h)
120	5.2018E-7
130	3.6009E-6
140	2.3540E-6
150	6.5662E-6
160	1.2703E-5
180	4.1193E-5

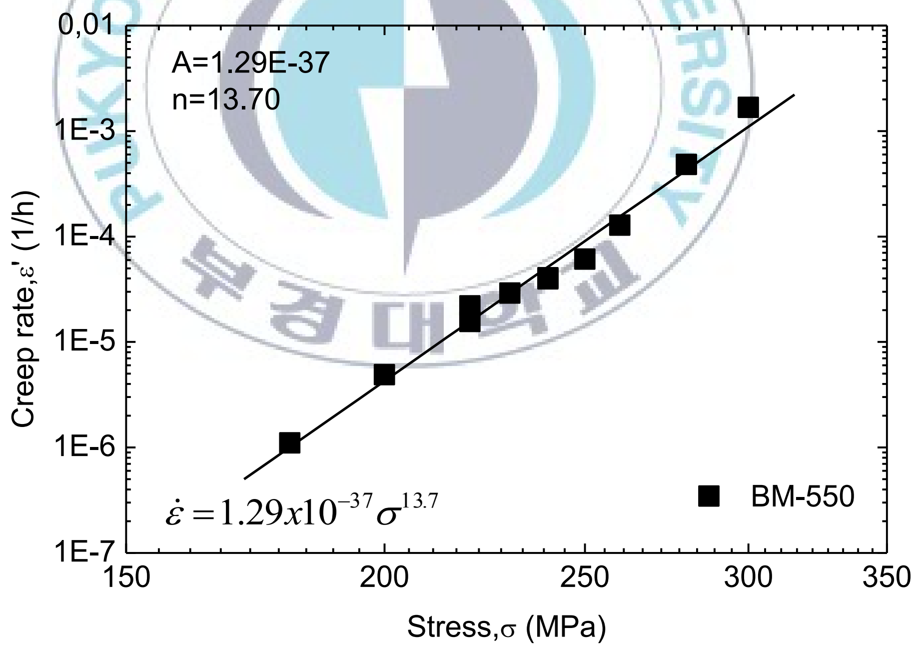

Figure 4 . 1 Determination of creep constants at 550°C.

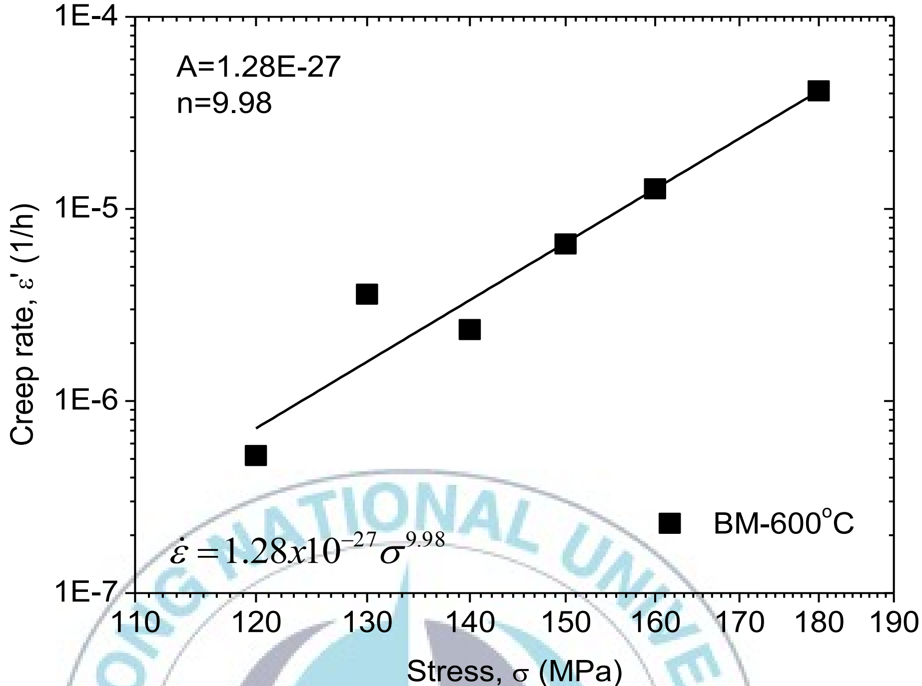

Figure 4 . 2 Determination of creep constants at 600°C.

4.2 Creep Crack Growth Rate Test Results

Figs. 4.3 and 4.4 show the ratio of load line displacement rates to total load line displacement rates, $(dV_c/dt)/(dV/dt)$ under various applied loads at 550°C and 600°C. The results show the ratio is more than 0.5, $(dV_c/dt)/(dV/dt) \geq 0.5$. It is obvious that the modified 9Cr-1Mo steel had a ductile characteristic. Therefore, the C^* parameter appropriates to characterize the CCGR for this steel. The transition time (t_T), from small scale to extensive creep by using Eq. (3.2) can be calculated for each point and the largest value of t_T is defined as the transition time.

The crack length and LLD obtained from the CCG tests are shown in Figs. 4.5 ~ 4.8. According to the measurement of potential difference, crack length a, was calculated using Eq. (3.1). It can be seen that the effects of increasing temperature or increasing stress are to raise the levels and shapes of the time.

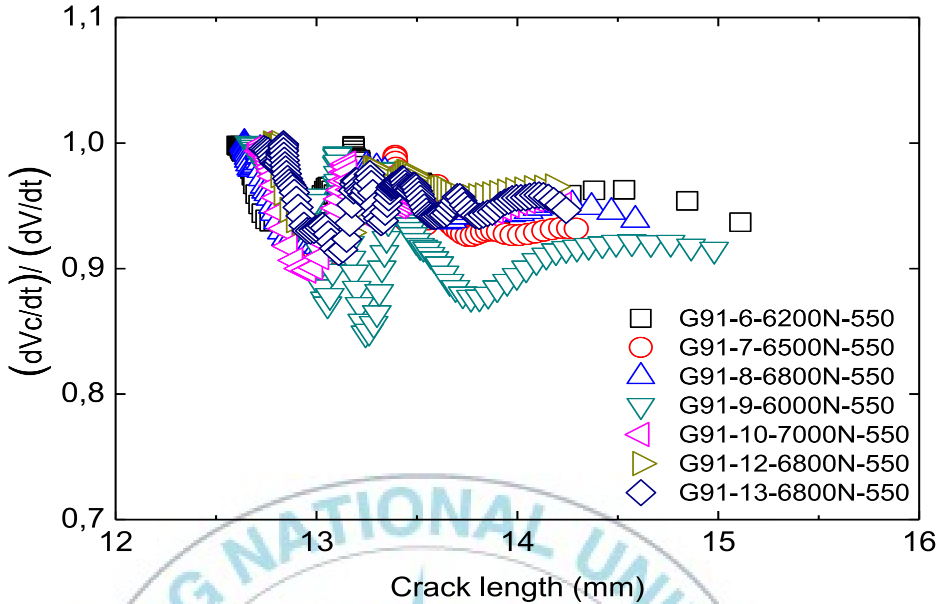

Figure 4 . 3 Validity criteria corelating to the CCG data with the parameter at 550^{o}C.

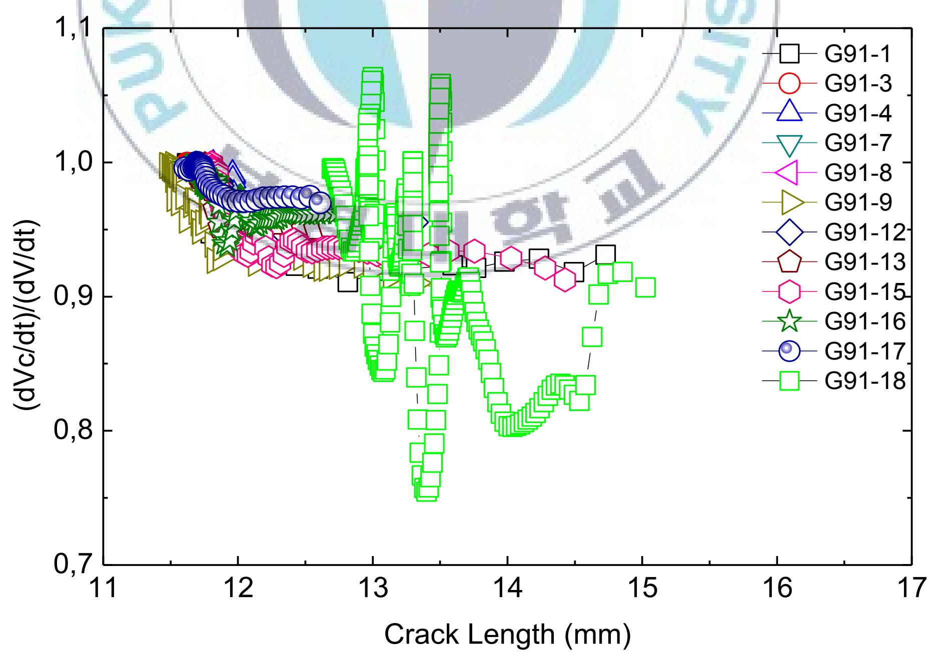

Figure 4 . 4 Validity criteria corelating to the CCG data with the parameter at 600^{o}C.

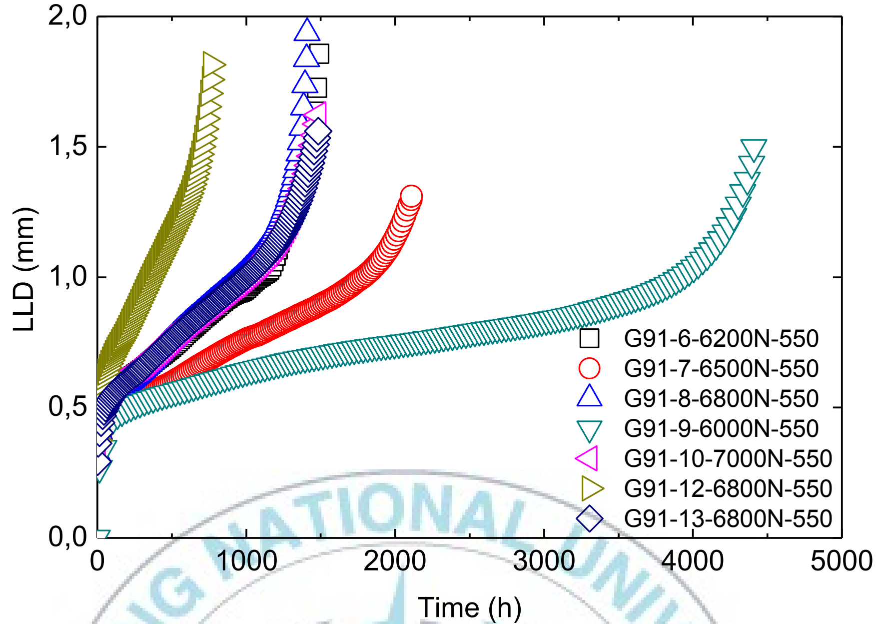

Figure 4 . 5 Plot of LLD vs. time at 550°C.

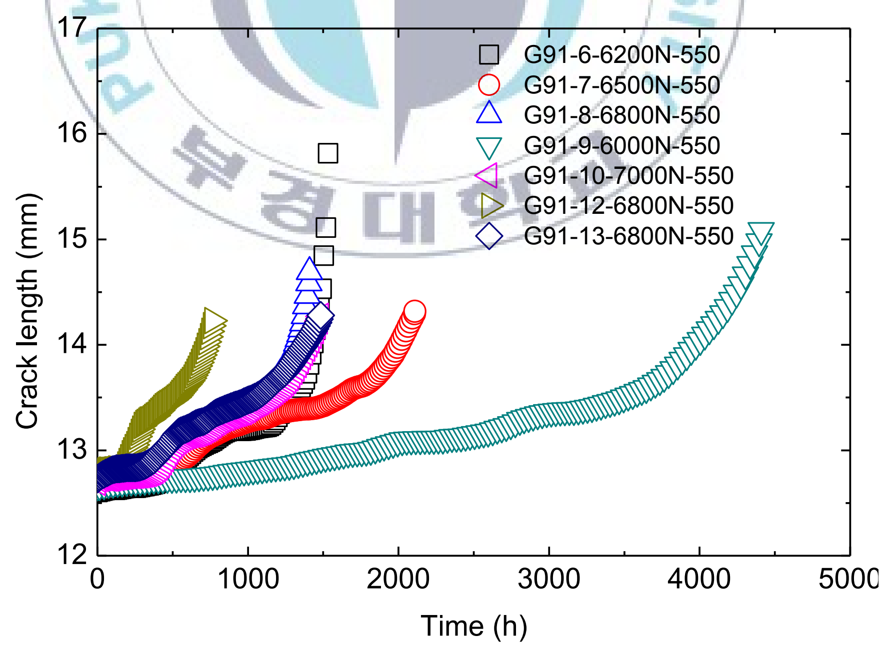

Figure 4 . 6 Plot of crack length vs. time at 550°C.

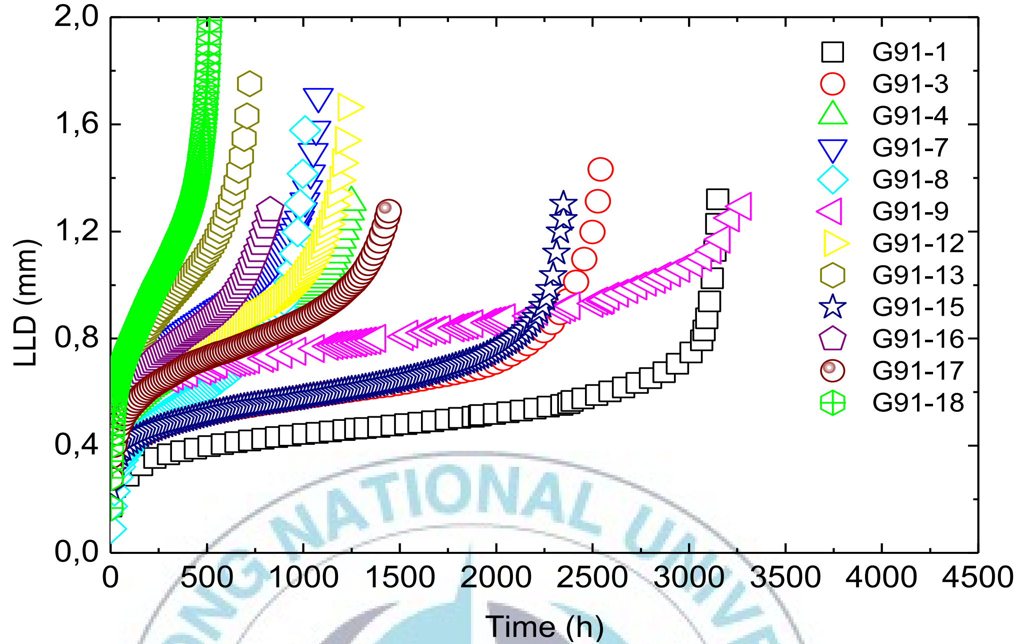

Figure 4 . 7 Plot of LLD vs. time at 600°C.

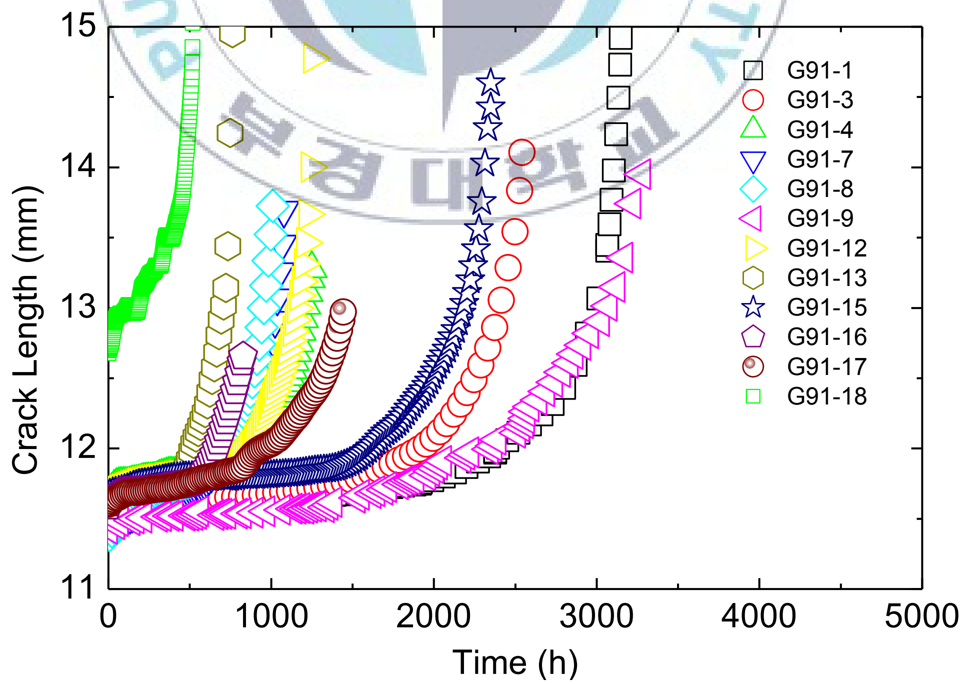

Figure 4 . 8 Plot of crack length vs. time at 600°C.

4.2.1 *K* Parameter

This parameter due to the supposition of the stress field near the crack tip that is controlled by linear fracture mechanics and the small-scale yielding condition. The *K*-values for the CT specimens were obtained from the following equation according to ASTM E-399 [33]:

$$K = \frac{P}{B^{1/2} B_N^{1/2} W^{1/2}} \left[\frac{2 + a/W}{(1 - a/W)^{3/2}} \right] f(a/W) \tag{4.3}$$

$$f(a/W) = 0.886 + 4.64\,a/W - 13.32(a/W)^2 + 14.72(a/W)^3 - 5.6(a/W)^4$$

In Fig. 4.9, the obtained results are evaluated by using stress intensity factor *K*. The relation of *da/dt* to *K* for the standard CT specimens seems to be devided into two groups of 550°C and 600°C. There is the large scatter in the CCGR data, and there is also no systematic trend among each series of test for this steel. It seems to be difficult to characterize the modified 9Cr-1Mo steel by the *K* parameter.The reason for this is because of a ductile material.

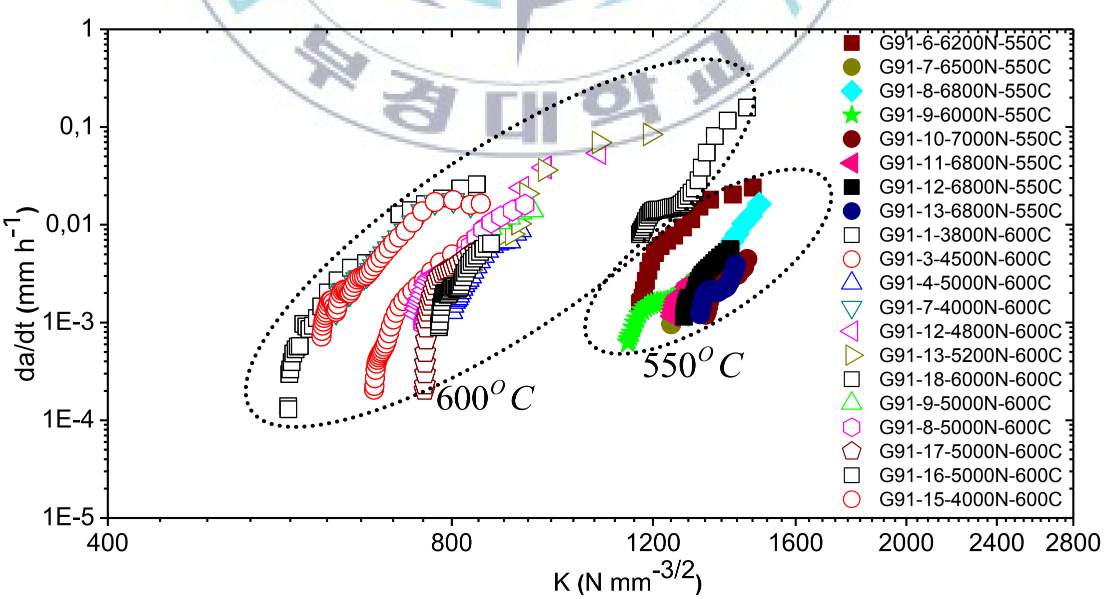

Figure 4 . 9 Determination of the CCGR with *K* parameter.

4.2.2 C^* Parameter

For the CT specimens, the C^* values were calculated by Eq. (4.4) given in ASTM standard E-1457 using experimental load line displacement rates and CCG data.

$$C^{*LLD} = \frac{P\dot{\Delta}^{C}}{B_n(W-a)} H^{LLD} \eta^{LLD} \tag{4.4}$$

The CCGR were found to be correlated to the C^*, i.e. by $da/dt=B[C^*]^q$, where B and q are the material constants under various load at 550°C and 600°C.

In Fig. 4.10 and. 4.11, the CCGR da/dt is ploted against C^*, calculated from LLD including the transition time at a specific temperature. In da/dt-C^* relation, the C^* values decreases in the early stage of crack growth and subsequently increase, i.e. a dual value due to nose. It is due to the fact that the CCGR has a different rate dependence from the displacement rate of the specimens at the early stages of crack propagation. This phenomena has been explained in chapter 2. Therefore, it should be considered when the early stage is regarded for some practical use.

Based on the validity criteria of ASTM standard E-1457, only data points that exceed the transition time t_T were considered to ensure the crack extension occuring under extensive creep condition. The transition time can be determined by using Eq. (3.2). Fig. 4.12 and 4.13 show the CCGR estimated by the C^* parameter under various load at 550°C and 600°C excluding transition time.

The correlation between the corresponding CCGR and the C^* values can be described by using $da/dt = B[C^*]^q$. By determining the values of the B and q, it is possible to calculate CCGR for a given C^* values. As shown in Fig. 4.12 and 4.13, a least square fitting method (LSFM) is used to determine the B and q values by taking the best linear regression of the total CCG data. The CCGR law at 550°C for the C^* was obtained as:

$$\frac{da}{dt} = 4.3784 \times 10^{-03} [C*]^{0.6799} \tag{4.5}$$

and the CCGR law at 600^{o}C was obtained as:

$$\frac{da}{dt} = 7.6015 \times 10^{-03} [C*]^{0.7913} \tag{4.6}$$

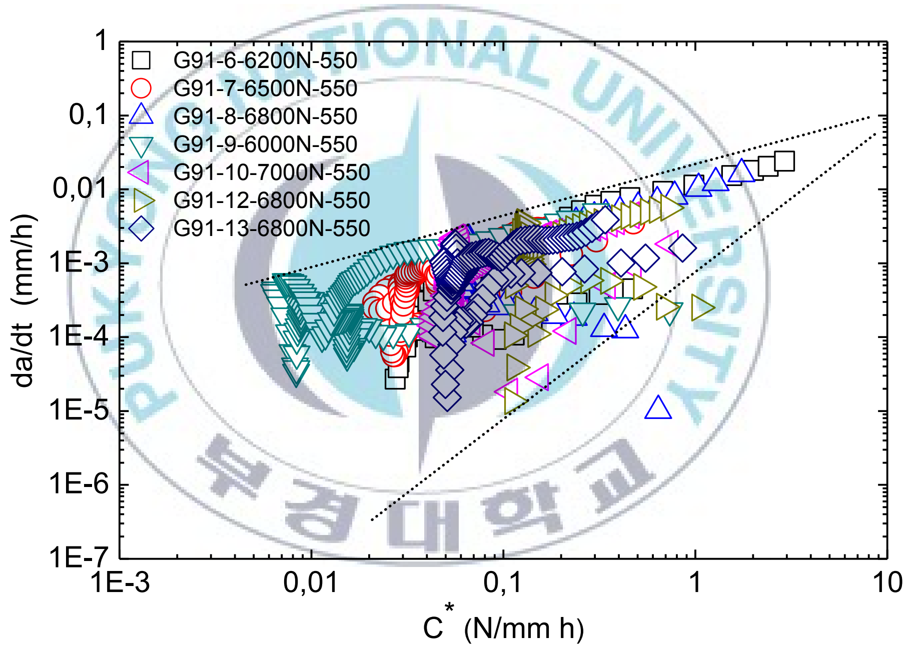

Figure 4 . 10 Plot of CCGR vs. C^* at 550^{o}C including transition time.

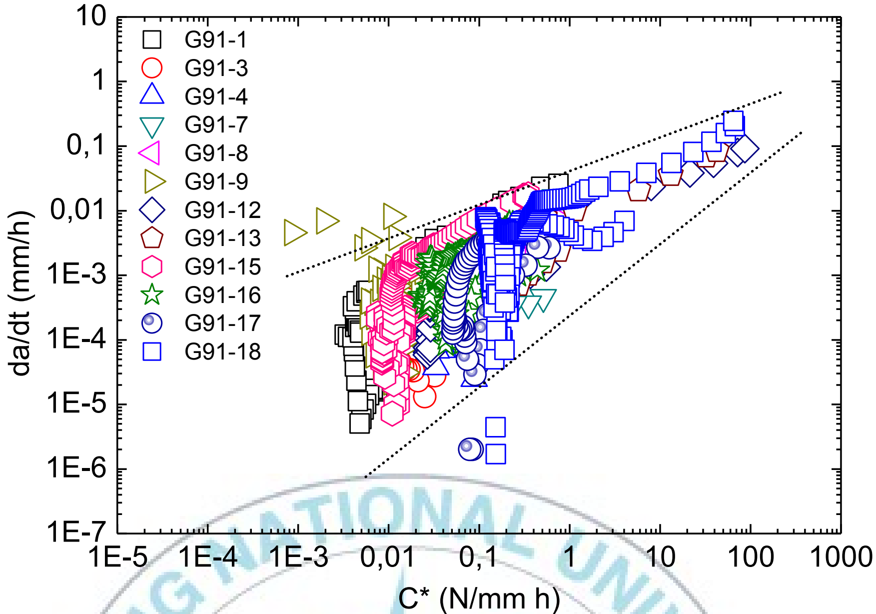

Figure 4 . 11 Plot of CCGR vs. C^* at 600°C including transition time.

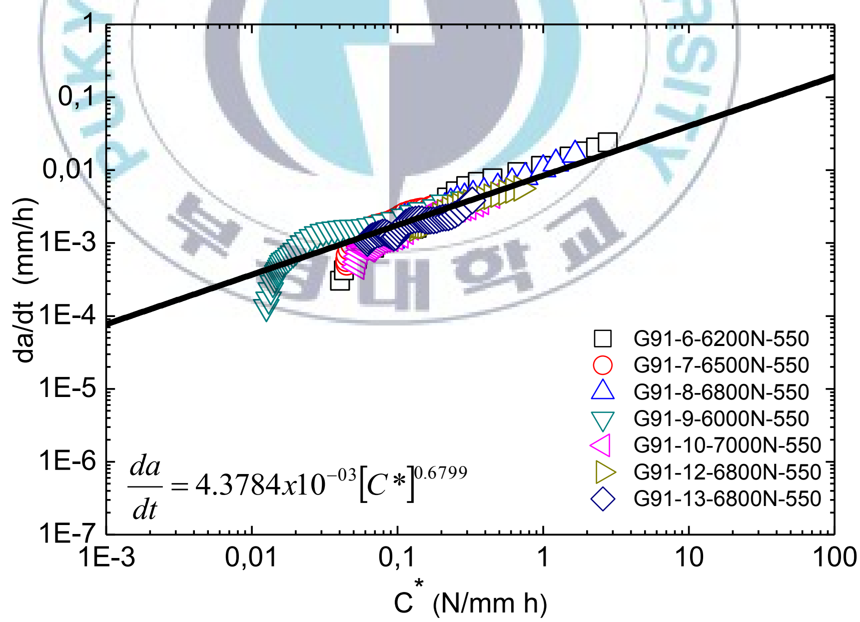

Figure 4 . 12 Result of CCGR law by the C^* at 550°C excluding transition time.

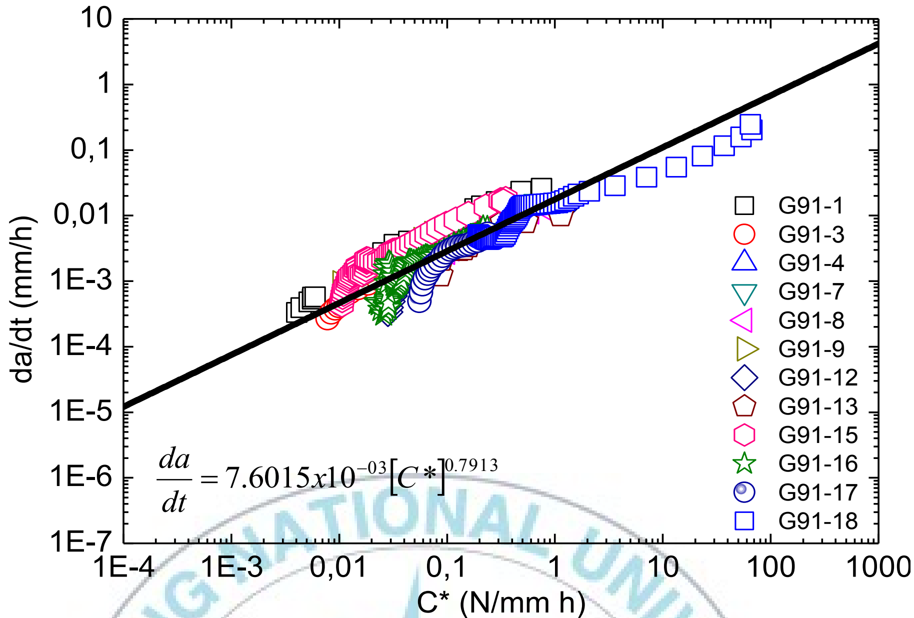

Figure 4 . 13 Result of CCGR law by the C^* at 600°C excluding transition time.

4.2.3 Q^* Parameter

The Q^* parameter in this study was used as an alternative parameter to analyze the CCGR of modified 9Cr-1Mo steel. Its CCGR can be expressed in term of an activation process equation, and the Q^* parameter was defined as the exponent of the exponential in the thermal activation process equation for *da/dt* in which the activation energy is expressed in terms of free energy, as follows:

$$\frac{da}{dt} = A^* \exp\left(-\frac{U}{RT}\right) \tag{4.7}$$

Under various stresses, the relation between absolute temperature T and CCGR *da/dt* which was characterized by the K parameter, as shown in Fig. 4.14, indicates an Arrhenius-type temperature dependence; i.e. with an increase in K-value, the absolute value of the gradient decreases, as shown in Fig. 4.15.

The creep exponent n versus the inverse of absolute temperature $1/T$ indicates a linearly increasing function, as shown in Fig. 4.16.

$$n = -51.251 + 53.455(1000/T) \tag{4.8}$$

The U value obtained from the tangent value of straight line in Fig. 4.17 according to Eq. (4.7) was proved to be expressed, as follows:

$$U = 251.465 - 174.436 \ln(K/1260.32) \tag{4.9}$$

In the second terms of this equation, 1260.32 $Nmm^{3/2}$ was determined experimentally to make the first terms of the activation energy equal to the self-diffusion energy.

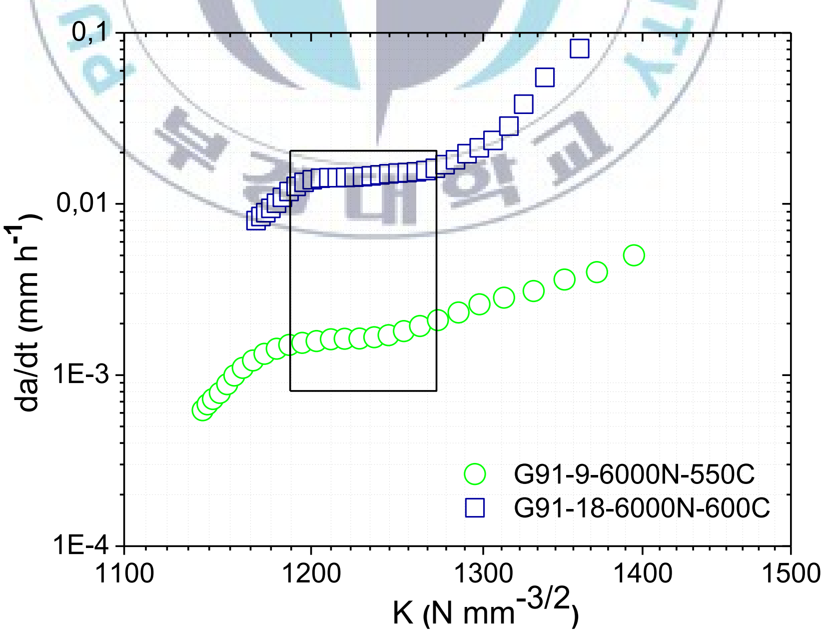

Figure 4 . 14 Determination of activation energy at a specific value of stress.

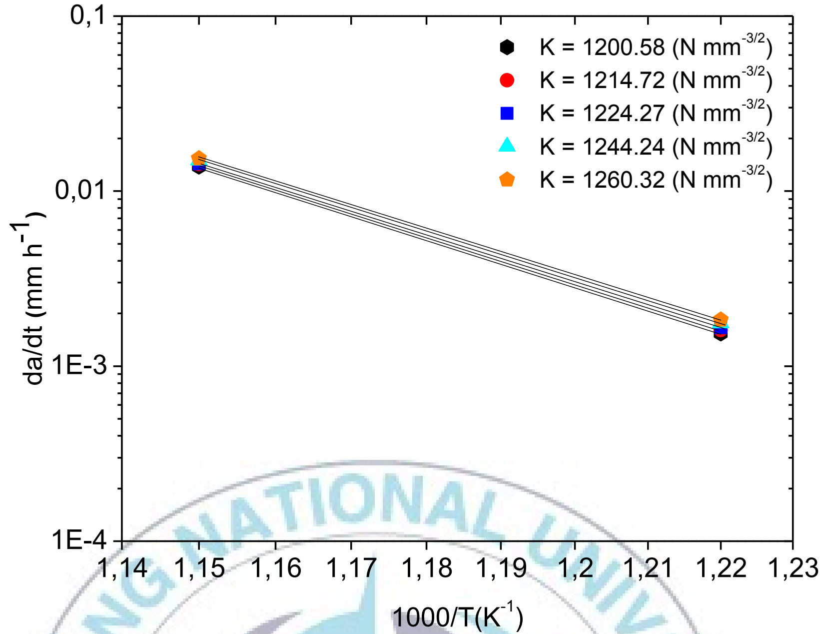

Figure 4 . 15 Relationship between the CCGR and inverse absolute temperature.

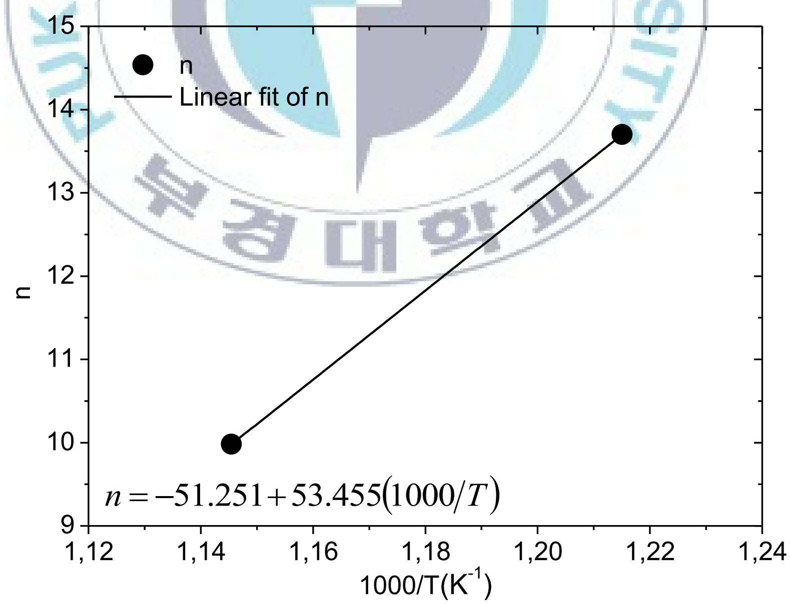

Figure 4 . 16 Relationship between the creep exponent and inverse of absolute temperature.

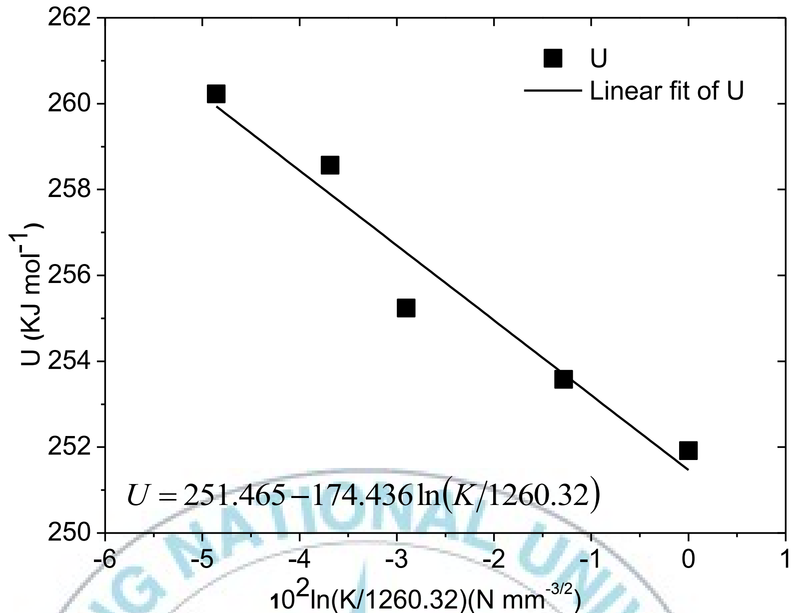

Figure 4 . 17 Relationship between the apparent activation energy *U* and the *K* parameter.

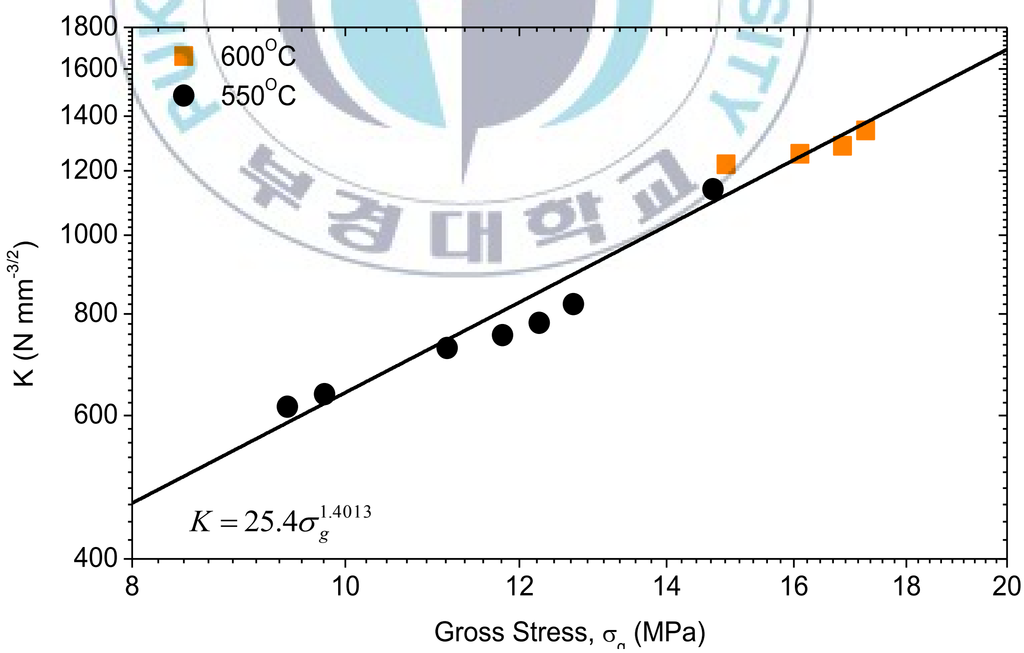

Figure 4 . 18 Relationship between the *K* and gross stress at a specific CCGR.

Based on the Eqs. (4.7) ~ (4.9), the creep crack growth rate was proved to be expressed in terms of K, σ_g, and T, as follows:

$$\frac{da}{dt} = 25.4\sigma_g^{1.4013}\left(\frac{K}{1260.32}\right)^{-51.25}\exp\left(-\frac{251.47+174.44\ln(K/1260.32)}{RT}\right) \qquad (4.10)$$

Concerning the variables σ_g and K of Eq. (4.10), the dependence on stress intensity factor K, is equal to the first terms of Eq. (4.8), and the dependence on gross stress σ_g, is obtained from the load dependence at the same temperature shown in Fig. 4.18, and thus Eq. (4.10) was derived.

The Q^* parameter could be derived on the basis of Eq. (4.10), as follows. By converting both sides of Eq. (4.10) into logarithms and substituting the gas constant:

$$\log\frac{da}{dt} = 1.405 + \left\{\frac{48.32x10^3}{T}\log\left(\frac{K}{5329.3}\right) - 51.2512\log\left(\frac{K}{1260.32}\right) + 1.4013\log\sigma_g\right\} \qquad (4.11)$$

the Q^* parameter is defined as exponent of the exponential function in the thermal activation process equation in which the activation energy. Therefore, the part of the brackets in Eq. (4.11) corresponds to the Q^* parameter. By defining this part as Q^*:

$$Q^* = \frac{48.32x10^3}{T}\log\left(\frac{K}{5329.3}\right) - 51.2512\log\left(\frac{K}{1260.32}\right) + 1.4013\log\sigma_g \qquad (4.12)$$

Fig. 4.19 shows the crack growth estimated by the Q^* parameter under various loads at 550°C and 600°C. The parameter can characterize the variation of the CCGR that occurs with the change of temperatures, and applied stress conditions in terms of independent parameter. Also, the parameter reveals a simple monotical linear function without a dual value due to nose at the early stage of the CCG curve.

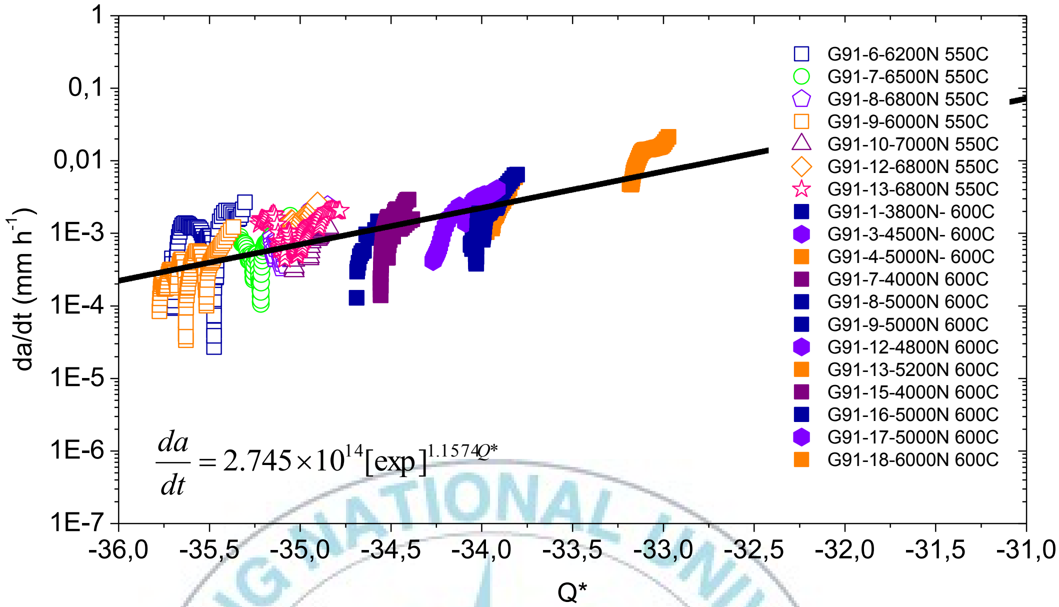

Figure 4 . 19 Determination of the CCGR by the Q^* parameter under various loads at 550°C and 600°C.

4.3 Comparison of Each Parameter

Fig. 4.20 shows the CCGR line evaluated by the C^* parameter. It shows the better agreement between the CCGR line in the distribution data and the experimental data under various loads at 550°C and 600°C than the K parameter, as shown in Fig. 4.9. As discussed above, the relationship between *da/dt* and K was divided into two groups at 550°C and 600°C. It is obvious that there was a large scatter and no systematic trend among each series of the tests.

In addition, in the *da/dt*-C^* relationship, the C^* decreases at the early stage of crack growth and subsequently increases, i.e. a dual value due to the nose appearance. The scatter can be seen to exist in data, especially at lower values of the C^*. The data are distributed to the upper C^* at 600°C and the lower C^* at 550°C. Therefore, the CCGR line can not be exactly located in the same band and formulated in the same equation under different temperatures. Also, the data shows that the *da/dt* is not exactly characterized by the C^* alone, because it depends on the creep deformation rate, which is a function of stresses and temperatures. It can be seen from Fig. 4.20 that such a stress or temperature variation can not be distinguished by the estimation of the C^*, which is involved in the same band.

It is obvious that the Q^* parameter can characterize the variation of the CCGR in terms of independent parameter, as shown in Fig. 4.19. The Q^* parameter is sensitive under various loads at 550°C and 600°C. This gives a straight line increasing or decreasing regardless of the testing conditions such as temperature and stress. Also, it gives a simple monotical linear function without a dual value due to nose at the early stage. The agreement between the CCGR line and the experimental data is valid, and the CCGR law was obtained as follows:

$$\frac{da}{dt} = 2.745\times10^{14}[\exp]^{1.1574Q^*} \tag{4.13}$$

where the B value was 2.745E14, and the m value was 1.1574.

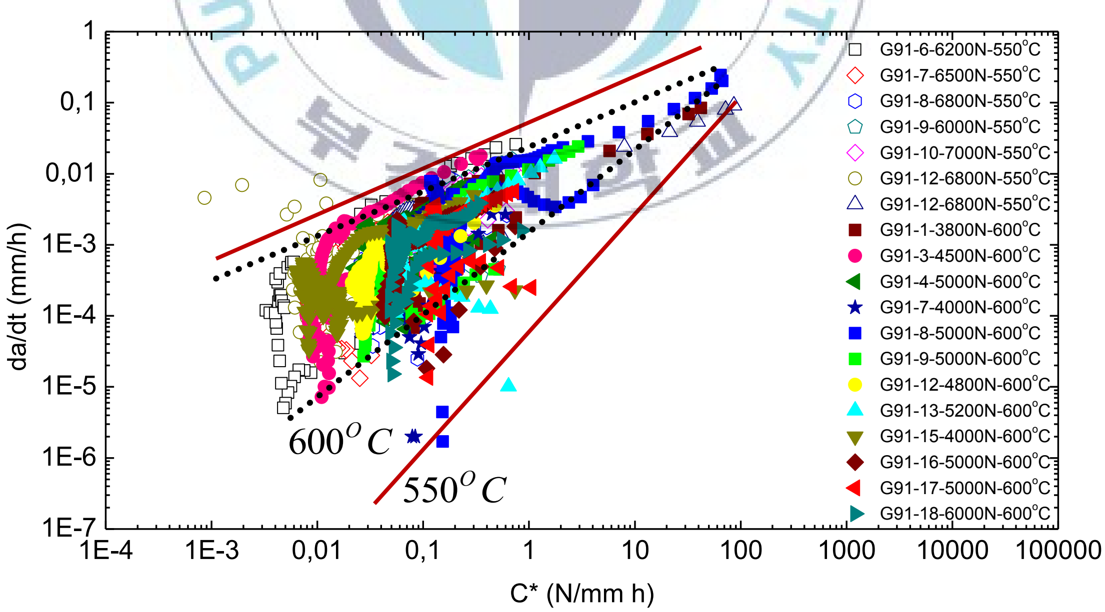

Figure 4 . 20 Determination of the CCGR by the C^* parameter under various loads at 550°C and 600°C.

V. Conclusions

To characterize the CCGR of the modified 9Cr-1Mo steel, which is considered as one of the major structural components for a Gen-IV reactors, the Q^* parameter in addition to the K and C^* parameters were considered. A series of creep and CCG tests was conducted under various applied loads at 550°C and 600°C, and using the obtained experimental data, the CCG behaviors for the K, C^*, and Q^* were investigated, and especially the evaluation of the Q^* parameter was focused and presented in detail. The CCGR laws for the C^* and Q^* parameters were proposed, and their characteristics were compared and discussed. Through this study, following results were drawn.

1. The CCGR law for the C^* parameter at 550°C was obtained as ;

$$\frac{da}{dt} = 4.3784 \times 10^{-03} [C*]^{0.6799}$$

   and at 600°C was obtained as ;

$$\frac{da}{dt} = 7.6015 \times 10^{-03} [C*]^{0.7913}$$

2. The CCGR law for the Q^* parameter at 550 °C and 600°C was unified into a monotical linear line equation as ;

$$\frac{da}{dt} = 2.745 \times 10^{14} [\exp]^{1.1574Q*}$$

3. The Q^* parameter could characterize the variation of the CCGR in terms of independent parameter, and it gave a straight line regardless of effects of testing

conditions such as temperatures and loads. It showed simple monotical linear function without a dual value due to nose at the early stage.

4. In da/dt-C^* relation, the C^* parameter decreased at the early stage of crack growth, and subsequently increased, i.e. a dual value due to nose appears. The scatter in data always was existed, and especially at lower values of the C^*. The reason for this was because the CCGR has a different rate from the displacement rate of the specimens at the early stages of crack propagation. It was identified that the C^* parameter was regarded as a dependent parameter that depends on creep deformation rate, which was a function of stress, temperature, specimen shape, and activation energy of deformation, etc.

5. It was found that the relationship of da/dt to K for standard specimens of modified 9Cr-1Mo steel was divided into two groups at 550°C and 600°C.

6. In the scattered data from the early stage to acceleration stage, the Q^* parameter was found to be superior to the C^* parameter, while the K parameter showed the largest scatter, and there was no systematic trend among each series of tests.

References

[1] Natesan, K., Purohit, A., and Tam, S. W., "Material Behavior in HTGR Environments", Argonne National Laboratory, Washington, DC, pp: 9 ~ 11, 2003.

[2] Kim, W. G., Park, J. Y., Hong, S, D., and Kim, S. J., "Probabilistic Assessment of Creep Crack Growth Rate for Gr.91 Steel", *Nucl. Eng.*, 241, pp: 3580-3586, 2011.

[3] Yokobori , Jr, A. T., Yokobori, T., Nishihara, T., and Yamaoka, T., "An Alternative Correlating Parameter for Creep Crack Growth Rate and Its Application: Derivation of The Parameter Q^*", *Materials at High Temperatures*, 10, pp: 108 ~ 118, 1992.

[4] Yokobori, T., Tanaka, C., Yagi, K., Kitagawa, M., Fuji, A., Yokobori , Jr, A. T., and Tabuchi, M., "Result of an Intercomparison of Creep Crack Growth Tests Made in Japan", *Materials at High Temperatures*, 10, pp: 97 ~ 107, 1992.

[5] Yokobori, Jr, A. T., and Yokobori, T., "Comparative Study on Characterization Parameters for High Temperature Creep Crack Growth With Special Emphasis on Dual Value Behavior of Crack Growth Rate", *Eng. Fract. Mech*, 55, pp: 493 ~ 503, 1996.

[6] Yokobori, T., Sakata, H., and Yokobori , Jr, A. T., "A New Parameter for Prediction of Creep Crack Growth Rate at High Temperature", *Eng. Fract. Mech,* 13, pp: 533 ~ 539, 1980.

[7] Yokobori, Jr, A. T., Tomizawa, Jr, H., Sakata, H., Kako, T., and Kuriyama, T., "Representation of The Displacement Rate Between The Loading Points in Terms Of Applied Stress and Temperature and Its Relation to Creep Crack Growth Rate, C^*, P and Q^* Parameters", *Eng. Fract. Mech*, 28, 805-816, 1987.

[8] Yokobori , Jr, A. T., Yokobori, T., Kuriyama, T,. Kako, T., and Kaji, Y., *Proc. Int. Conf. Creep*, JSME, IME, ASME, ASTM, pp: 135, 1986.

[9] Kaji, Y., Kikuchi, K., and Yokobori , Jr, A. T., "Estimation of Creep Fracture

Life for Hastelloy XR by *Q** Parameter", *Eng. Fract. Mech.* 50, pp: 519 ~ 528, 1995.

[10] Yokobori , Jr, A. T., Yokobori, T,. and Nishihara, T,. "Characterization of High Temperature Creep Crack Growth and Creep Life From High Temperature Ductile Through to High Temperature Brittle Materials", *Eng. Fract. Mech*. 40, pp: 737 ~ 748, 1991.

[11] Yokobori , Jr, A. T., Tomoharu, U., Yokobori, T,. Akio, F., Masaki, K., Isamu, Y., Masaaki, T., and Koichi, Y., "Estimation of creep crack growth rate in IN-100 based on the *Q** parameter concept", *Journal of Material Science,* 33, pp: 1555 ~ 1562, 1998.

[12] Saxena, A.," Nonlinear Fracture Mechanics for Engineers", CRC Press, NY, pp: 363~ 377, 1997.

[13] Rice, J. R., "A Path Independent Integral and Approximate Analysis of Strain Concentration by Notches and Cracks", *Journal of Applied Mechanics, Transaction of the ASME*, 35, pp: 379 ~ 386, 1968a.

[14] Rice, J. R., and Rosengren, G. F., "Plain Strain Deformation Near a Crack Tip in Power Law Hardening Material", *Journal of Applied Mechanics and Physics of solids,* 16, pp: 1 ~ 12, 1968b.

[15] Nikbin, K. M., Smith, D. J., and Webster, G. A., "Prediction of Creep Crack Growth from Uniaxial Creep Data", *Proceedings of the Royal Society,* A396, pp: 183 ~ 197, 1984.

[16] Wesbster, G. A., "Methods of Measuring Crack Growth at Elevated Temperatures", *Measurement of High Temperature Mechanical Properties of Materials,* pp: 255 ~ 277, 1992.

[17] Webster, G. A., and Ainsworth, R. A., "High Temperature Component Life Assessment", 1st ed. Cambridge: Chapman and Hall, pp: 110 ~ 125, 1994.

[18] ASTM A-826 - 88, "Standard Specification for Austenitic and Ferritic Stainless Steel Duct Tubes for Breeder Reactor Core Components", 1988.

[19] Irwin, G. R., "Analysis of Stresses and Strains Near the End of a Crack

Transversing a Plate", *Journal of Applied Mechanics,* 25, pp: 361 ~ 364, 1957.

[20] Williams, M. L., "On the Stress Distribution at the Base of Stationary Crack", *Journal of Applied Mechanics*, 24, pp. 109 ~ 114, 1957.

[21] Anderson, T. L., "Fracture Mechanics 2nd Edition", CRC Press, Boca Raton, Ann Arbor, London, Tokyo, pp: 31 ~ 245, 1995.

[22] Davies, C. M., Kourmpetis, M., O'Dowd, N. P., and Nikbin, K. M., "Experimental Evaluation of the *J* or *C** Parameter for a Range of Cracked Geometries", *Journal of ASTM International,* 2006, 3, pp: 1 ~ 20, 2006.

[23] Anderson, T. L., "Fracture Mechanics and Applications" 3rd Edition", CRC Press, Boca Raton, Ann Arbor, London, Tokyo, CRC Press, pp: 205 ~ 255, 2005.

[24] Ashby, M. F., and Jones, D. R. H., "Engineering Materials 1: An Introduction to Their Properties and Applications", Butterworth Heinemann., 1, pp: 10 ~ 100, 1996.

[25] Frost, H. J., and Ashby, M. F., "Deformation Mechanism Maps", Oxford, pp: 1 ~ 20, 1982.

[26] Riedel, H., and Rice, J. R., "Tensile Cracks in Creeping Solids", *Paper Presented at Fracture Mechanics,* St-Louis, 34, pp: 112 ~ 130, 1980.

[27] Landes, J. D., and Begley, J. A., "A Fracture Mechanics Approach to Creep Crack Growth", *ASTM STP 590,* pp: 128 ~ 148, 1976.

[28] ASTM E-139-11, "Standard Test Method for Conducting Creep, Creep-Rupture and Stress Rupture Tests of Metallic Materials", 2011.

[29] Aronson, G. H., and Ritchie, R. O., "Optimisation of the Electrical Potential Technique for Crack Growth Monitoring in Compact Test Pieces Using Finite Element Analysis", *Journal of Testing and Evaluation,* 7, pp: 208 ~ 215, 1979.

[30] Wei, R. P., and Brazill, R. L., "An Assessment of A.C. and D.C. Potential Systems for Monitoring Fatigue Crack Growth", *ASTM STP 738*, pp: 103 ~ 119, 1981.

[31] Hicks. M. A., and Pickard, A. C., "A Comparison of Theoretical and Experimental Methods of Calibrating the Electrical Potential Drop Technique for

Crack Length Determination", *International Journal of Fracture,* 20, pp: 91 ~ 101, 1982.

[32] ASTM E-1457-07, "Standard Test Method for Measurement of Creep Crack Growth Rates in Metals", 2007.

[33] ASTM E-399-12e1, "Standard Test Method for Linear-Elastic Plane Strain Fracture Toughness K_{Ic} of metallic materials", 2012.

Acknowledgment

Two years have passed since I joined to the Smare Lab. During this period, I am indebted to many persons. I would like to first thank Prof. Seon-Jin Kim and Dr. Woo-Gon Kim, who advised me through my graduate work. They gave countless words of advice on the technical aspects of my research and taught me with passion and love. I would also like to thank Prof Yeung-Sik Kim for giving me a lot of valuable knowledge on material science, I also express my thanks for the support and service on my graduate committee. Their advice on my research was invaluable.

I would like to thank the members of my laboratory: Jae-Young Park (especially for helping and teaching me about experiments), Yeui-Han Jeong, Phil-Ho Choi, for their help, support and useful discussions.

My special thanks must go on to Dr. Gunawan Dwi Haryadi, Dr. Stenly Tangkuman, Pandu Sandi Pratama, Bangun Irham and many others. Because of them, I was able to face the 'nonlinearities' of my life in Korea.

Most importantly, I am particularly grateful to my parents and my brother. Without their support and help, the hard process of my study would not have been completed. And last, but certainly not least, I would like to thank my honey, Sang Ayu Putu Piastini Gunaasih, for her endless love, her great understanding and for the motivation that she gave to me continuously although she did not know what I did.